

Journal Pre-proofs

Synthesis, biological evaluation, and molecular docking analysis of phenstatin based indole linked chalcones as anticancer agents and tubulin polymerization inhibitors

Jyoti Kode, Jeshma Kovvuri, Burri Nagaraju, Shailesh Jadhav, Madan Barkume, Subrata Sen, Nirmal Kumar Kasinathan, Pradip Chaudhari, Bhabani Shankar Mohanty, Jitendra Gour, Dilep Kumar Sigalapalli, C. Ganesh Kumar, Trupti Pradhan, Manisha Banerjee, Ahmed Kamal

PII: S0045-2068(20)31745-4
DOI: <https://doi.org/10.1016/j.bioorg.2020.104447>
Reference: YBIOO 104447

To appear in: *Bioorganic Chemistry*

Received Date: 1 April 2020
Revised Date: 27 October 2020
Accepted Date: 28 October 2020

Please cite this article as: J. Kode, J. Kovvuri, B. Nagaraju, S. Jadhav, M. Barkume, S. Sen, N. Kumar Kasinathan, P. Chaudhari, B. Shankar Mohanty, J. Gour, D. Kumar Sigalapalli, C. Ganesh Kumar, T. Pradhan, M. Banerjee, A. Kamal, Synthesis, biological evaluation, and molecular docking analysis of phenstatin based indole linked chalcones as anticancer agents and tubulin polymerization inhibitors, *Bioorganic Chemistry* (2020), doi: <https://doi.org/10.1016/j.bioorg.2020.104447>

This is a PDF file of an article that has undergone enhancements after acceptance, such as the addition of a cover page and metadata, and formatting for readability, but it is not yet the definitive version of record. This version will undergo additional copyediting, typesetting and review before it is published in its final form, but we are providing this version to give early visibility of the article. Please note that, during the production process, errors may be discovered which could affect the content, and all legal disclaimers that apply to the journal pertain.

© 2020 Published by Elsevier Inc.



Synthesis, biological evaluation, and molecular docking analysis of phenstatin based indole linked chalcones as anticancer agents and tubulin polymerization inhibitors

Jyoti Kode^{*,a,b,c,@}, *Jeshma Kovvuri*^{d,e,j,@}, *Burri Nagaraju*^{d,e,@}, *Shailesh Jadhav*^a, *Madan Barkume*^a, *Subrata Sen*^a, *Nirmal Kumar Kasinathan*^a, *Pradip Chaudhari*^{c,f}, *Bhabani Shankar Mohanty*^f, *Jitendra Gour*^g, *Dilep Kumar Sigalapalli*^g, *C. Ganesh Kumar*^{d,e}, *Trupti Pradhan*^b, *Manisha Banerjee*^{c,h} and *Ahmed Kamal*^{*,d,e,g,i,@}

^aAnti-Cancer Drug Screening Facility (ACDSF), ^bTumor Immunology & Immunotherapy Group, Advanced Centre for Treatment, Research & Education in Cancer (ACTREC), Tata Memorial Centre, Kharghar, Navi Mumbai 410210, India

^cHomi Bhabha National Institute (HBNI), Training School Complex, Anushakti Nagar, Mumbai 400085, India

^dDepartment of Organic Synthesis and Process Chemistry, CSIR-Indian Institute of Chemical Technology, Hyderabad 500 007, India

^eAcademy of Scientific and Innovative Research (AcSIR), New Delhi 110025, India

^fSmall Animal Imaging Facility, Advanced Centre for Treatment, Research & Education in Cancer (ACTREC), Tata Memorial Centre, Kharghar, Navi Mumbai 410210, India

^gDepartment of Medicinal Chemistry, National Institute of Pharmaceutical Education and Research (NIPER), Hyderabad 500 037, India

^hMolecular Biology Division, Bhabha Atomic Research Centre, Trombay, Mumbai- 400 085, India.

ⁱSchool of Pharmaceutical Education and Research (SPER), Jamia Hamdard, New Delhi 110062, India

^jDepartment of Humanities and Sciences, Vardhaman College of Engineering (Autonomous), Shamshabad, Hyderabad, Telangana, 501218, India

@The authors contributed equally.

* Corresponding authors

ABSTRACT:

A library of new phenstatin based indole linked chalcone compounds (**9a-z** and **9aa-ad**) were designed and synthesized. Of these, compound **9a** with 1-methyl, 2- and 3-methoxy substituents in the aromatic ring was efficacious against the human oral cancer cell line SCC-29B, spheroids, and in a mouse xenograft model of oral cancer AW13516. Compound **9a** exhibited anti-cancer activity through disrupting cellular integrity and affecting glucose metabolism-which is a hallmark of cancer. The cellular architecture was affected by inhibition of tubulin polymerization as observed by an immunofluorescence assay on **9a**-treated SCC-29B cells. An *in vitro* tubulin polymerization kinetics assay provided evidence of direct interaction of **9a** with tubulin. This physical interaction between tubulin and compound **9a** was further confirmed by Surface Plasmon Resonance (SPR) analysis. Molecular docking experiments and validations revealed that compound **9a** interacts and binds at the colchicine binding site of tubulin and at active sites of key enzymes in the glucose metabolism pathway. Based on *in silico* modeling, biophysical interactions, and pre-clinical observations, **9a** consisting of phenstatin based indole-chalcone scaffolds, can be considered as an attractive tubulin polymerization inhibitor candidate for developing anti-cancer therapeutics.

KEYWORDS:

Phenstatin based indole-linked chalcones; *in vitro* cell cytotoxicity; Cancer stem- like cells. Spheroid assay, oral cancer xenograft model; PET-CT imaging, ¹⁸F-fluorodeoxyglucose uptake, glucose metabolism; *in silico* analysis; molecular docking; tubulin polymerization inhibition; Surface Plasmon Resonance, multi-target metabolic inhibitor; anti-cancer efficacy, immunofluorescence, laser confocal microscopy, transmission electron microscopy.

INTRODUCTION:

Oral cancer is a debilitating cancer that ranks sixth in global occurrence. Oral squamous cell carcinoma (OSCC) is the most common malignant epithelial neoplasm affecting the oral cavity and it accounts for more than 90% of all oral cancers.¹ Microtubules are dynamic polymers of α - and β -tubulin dimers that play a pivotal role in the cell architecture, cellular processes, and cell division. Microtubule disruption can induce cell cycle arrest in G₂/M phase and abnormal mitotic spindle formation.² Moreover, tubulin inhibitors can also act as vascular disrupting agents.³⁻⁵ Hence tubulin polymerization inhibitors are one of the most important tools for drug discovery.^{6,7} Anti-tubulin agents such as vinca alkaloids, taxane and colchicine (Figure 1, (1)) bind to one of the three binding sites on tubulin subunits. It is believed that colchicine binding site tubulin inhibitors may be better than the other two site binders in overcoming drug resistance.⁸⁻¹⁰ They exhibit antiangiogenic property either by microtubule stabilization (e.g. docetaxel, taxanes)¹¹ or by destabilization (e.g. colchicine, combretastatins).¹² The present study is focused on the design of new tubulin polymerization inhibitors that act through blocking active colchicine binding site.

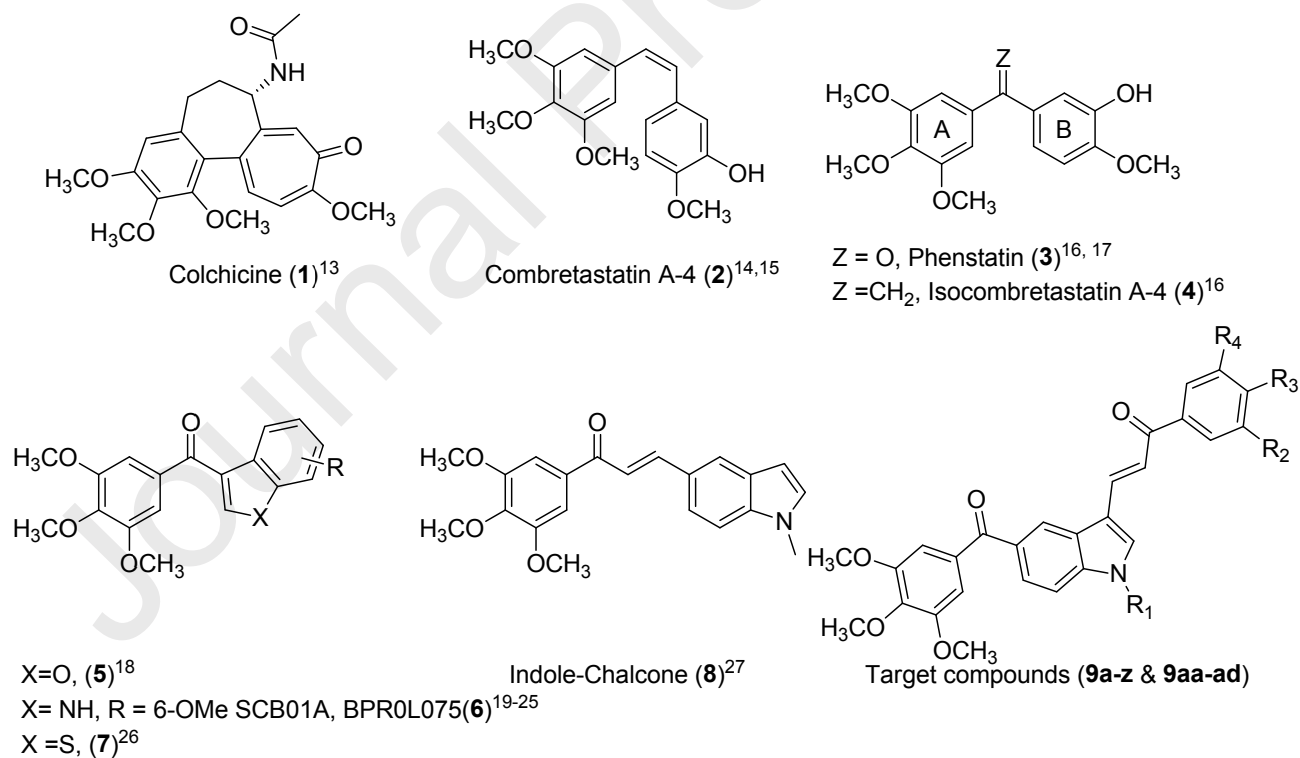


Figure 1. Chemical structures of some pharmaceutically important tubulin polymerization inhibitors including target compounds **9a-z** and **9aa-ad**.

Combretastatin A-4 (CA-4)²⁸ (Figure 1, **(2)**) is one of the most important naturally occurring tubulin polymerization inhibitor that binds to the colchicine site (Figure 1, **(2)**). **CA-4** analogs were synthesized and evaluated for their activity because of its simple structure. Based on the previous reports, the replacement of double bond in **CA-4** with sp^2 hybridized carbonyl group provides molecules like phenstatin (Figure 1, **(3)**), that will maintain the *cis* orientation of the two rings, a characteristic feature of **CA-4**, which is responsible for exhibiting better biological activities.¹⁷ Several phenstatin related compounds were synthesized, while retaining 3,4,5-timethoxyphenyl ring and by changing either B-ring with different heteroaromatic rings such as benzofuranyl (Figure 1, **(5)**), indolyl (Figure 1, **(6)**), benzothiophenyl (Figure 1, **(7)**) or by bridging with a methylene functionality (**4**). Among them, a compound with carbonyl bridge and indolyl B-ring (Figure 1, **(6)**) is known to efficiently inhibit cancer cell growth as well as tubulin polymerization.²⁹⁻³¹ Moreover, indole is a well-known privileged scaffold and its derivatives have been reported to exhibit a number of biological properties including anticancer activity.³²

On the other hand, chalcone is the privileged scaffold and one of the important core moieties of many naturally occurring biologically active compounds and has attracted much research attention in the recent past. In recent trend analysis, chalcone was reported by Zdrzil and Guha (2018)³³, as on the third position as a popular choice in the medicinal chemistry literature, after biphenyl and diphenyl ether. Several synthetic (Figure 1, **(8)**) and naturally occurring chalcones have been reported to possess significant anti-tubulin activities.^{27,34-38} These compounds are known to exhibit various biological activities including anti-malarial, anti-tubercular, anti-HIV apart from anticancer.³⁹ As a crucial example, penta-OMe-chalcone was found to overcome the drug resistance against the Vismodegib-resistant mutant G protein-coupled receptor Smoothed.⁴⁰ In the last few years, we have previously designed and synthesized a large number of conjugates and hybrids involving heterocyclics particularly based on combretastatin A-4, chalcones, and indoles in pursuit of newer, more effective and safer anticancer agents.⁴¹⁻⁴⁴ Considering these modifications and the biological importance of phenstatin, indole, and

chalcone scaffolds, we designed and synthesized phenstatin based indole linked chalcones to conserve the privileged structures of indole and trimethoxyphenyl. The resulted compounds were evaluated for their antiproliferative activity.

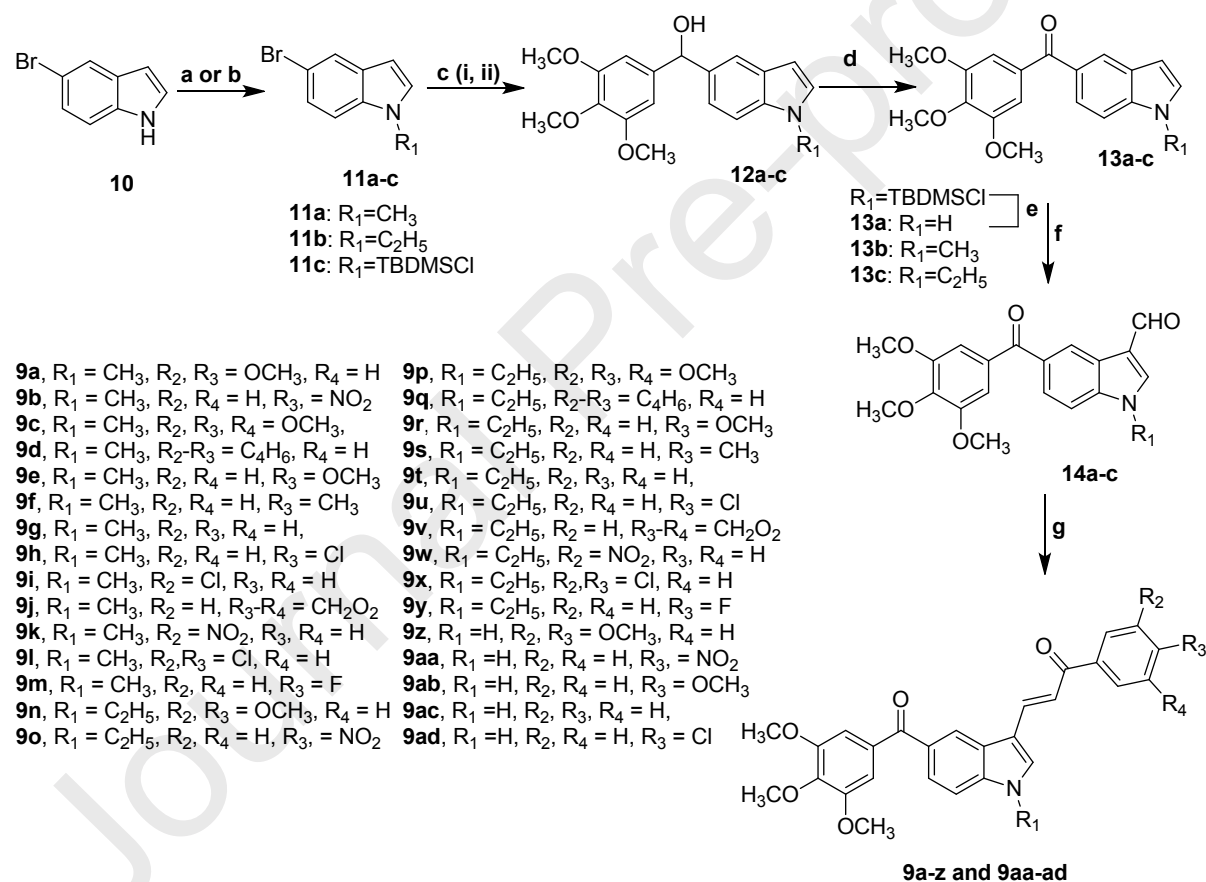
Increased glucose metabolism is considered a hallmark of cancer growth and progression.^{45,46} Cancer cells utilize aerobic glycolysis rather than oxidative phosphorylation termed as “Warburg effect”, which leads to faster glucose metabolism for ATP generation. This property of rapid glucose uptake is utilized for evaluating the effect of potential anti-cancer compounds as a response to therapy by tumor visualization using [¹⁸F]-fluorodeoxyglucose (¹⁸F-FDG) positron emission tomography/computed tomography (PET-CT) imaging. Hexokinase-2 (HK2) enzyme which marks the first catalytic step of glucose metabolism, is considered an important target of metabolic inhibitors that are designed as potential anti-cancer compounds.⁴⁵ Fenbendazole, a new microtubule interfering agent was found to display anti-neoplastic efficacy *in vitro* as well as *in vivo* through blocking the activity of HK2 enzyme- a key glycolytic enzyme. Fenbendazole was further found to act through multiple cellular pathways leading to the effective elimination of cancer cells, hence was considered as a potential therapeutic agent for cancer⁴⁷. Besides the glycolytic pathway, the tricarboxylic acid cycle (TCA) cycle also contributes to altered bioenergetic metabolism. Hence current efforts are focused on designing and identifying chemical compounds that have inhibitory action against multiple enzymes in glycolytic pathway and alternative energy pathway viz. TCA cycle. Based on this, in current study, biologically efficacious compounds were also evaluated for their efficacy to target glucose uptake by PET-CT study. Further advanced laser confocal microscopy imaging, *in silico* molecular docking tools, *in vitro* tubulin polymerization assay, and a biophysical tool like Surface Plasmon Resonance (SPR) were used to characterize molecular interactions of potential anti-cancer compounds with the active site of tubulin.

1. RESULTS AND DISCUSSION:

2.1. Chemistry

Phenstatin based indole linked chalcones (**9a-z** and **9aa-ad**) were synthesized as shown in Scheme 1. Initially, the *N*-substituted-5-bromoindoles **11a-c** were synthesized by *N*-alkylation

reaction of 5-bromoindole (**10**) with MeI and EtBr or by protecting with TBDMSCl in the presence of sodium hydride and DMF. This upon treatment with *n*-BuLi and 3,4,5-trimethoxybenzaldehyde in dry THF at -78°C yielded the corresponding secondary alcohols **12a-c** as shown in Scheme 1. Oxidation of **12a-c** with IBX in DMSO provided the keto compounds (**13a-c**). Thereafter the **13a** compound TBDMS group was deprotected using TBAF. Later **13a-c** compounds were subjected to Vilsmeier formylation to afford 1-methyl-5-(3,4,5-trimethoxybenzoyl)-1*H*-indole-3-carbaldehydes (**14a-c**) in good yields. Finally, the synthesized aldehydes were subjected to Claisen-Schmidt condensation with respective substituted acetophenones to afford the desired products, **9a-z** and **9aa-ad**. All the synthesized compounds were characterized by ^1H , ^{13}C NMR, and HRMS spectral analysis.



Scheme 1: Reagents and conditions: (a) TBDMSCl, NaH, THF, 0°C -rt, 3 h, 82%; (b) MeI/EtBr, NaOH, DMSO, 0°C -rt, 3 h, 91-93%; (c) i) THF, -78°C , *n*-BuLi, 1 h; ii) 3,4,5-trimethoxybenzaldehyde (in THF), 4 h, 72-76%; (d) IBX, DMSO, 0°C -rt, 3 h, 92-95%; (e) TBAF, THF, 0°C -rt, 4 h, 84% (f) POCl₃, DMF, CHCl₃, reflux, 12 h, 76-84%; (g) substituted acetophenone (1 eq), EtOH, 10% NaOH (aq.), rt, 6 h, 78-89%.

2.2. Biology

2.2.1. Cytotoxicity assay

To evaluate the biological usefulness of phenstatin based indole linked chalcones, these compounds were tested against some cancer cell lines of different tissue origins. The *in-vitro* testing of all these compounds was conducted at concentrations 0.1, 1, 10, and 100 μM by standard Sulforhodamine B (SRB) assay. Percent control growth was calculated and chemosensitivity response parameters GI_{50} (50% growth inhibition), TGI (total growth inhibition), and LC_{50} (50% lethal concentration) were extrapolated for all the compounds. Cell control was considered as 100% cell growth, Adriamycin (ADR) was considered as positive control and exhibited a lytic effect on cells seeded i.e. -50% cell growth.

As per NCI guidelines GI_{50} value of $\leq 10^{-6}$ M (i.e. 1 μM) was considered to demonstrate highly significant inhibitory activity in case of pure compounds. Compound **9b** (R_1 is methyl and R_3 is nitro) demonstrated significant anti-proliferative activity against Hep-G2 liver hepatoma cells, compound **9a** (R_1 is methyl, R_2 and R_3 are methoxy substituents, Supplementary Figure S1) against SCC-29B oral cancer cells and compounds **9e** (R_3 is methoxy) and **9l** (R_2 and R_3 are chloro substituents) against HT-29 colon cancer cells (Table 1). The structure activity relationship of the synthesized compounds indicated that the presence of trimethoxy ring and carbonyl group essential for tubulin activity and methoxy substituents at R_2 and R_3 enhanced cytotoxic activity (Supplementary Figure S1). We observed a few compounds exhibited moderate activity with $\text{GI}_{50} \leq 10\mu\text{M}$ and few demonstrated low activity with GI_{50} at $\leq 100\mu\text{M}$. It was observed that SCC-29 B oral cancer cell line was found to be sensitive target for most of the synthesized compounds (21 of 30) exhibiting low, moderate, or significant anti-proliferative activity. Hence this oral cancer cell line model was further utilized for spheroid assay too.

Table 1: *In vitro* cytotoxicity testing of the synthetic compounds against a panel of cancer cell lines by SRB assay

Sample Code	GI ₅₀ (μM)			Sample Code	GI ₅₀ (μM)		
	HEP-G2	SCC-29B	HT-29		HEP-G2	SCC-29B	HT-29
9a	>100	< 0.1	51	9q	>100	>100	>100
9b	0.018	88	43	9r	>100	>100	>100
9c	6.8	1.4	15	9s	>100	>100	>100
9d	6.5	1.6	5.2	9t	>100	59	>100
9e	11	1.2	< 0.1	9u	>100	>100	>100
9f	>100	1	>100	9v	>100	>100	>100
9g	>100	6.4	>100	9w	>100	>100	>100
9h	>100	17	>100	9x	>100	32	>100
9i	>100	>100	>100	9y	>100	64	>100
9j	>100	19	>100	9z	>100	>100	>100
9k	>100	>100	>100	9aa	>100	56	>100
9l	>100	59	< 0.1	9ab	>100	8.9	>100
9m	>100	11	>100	9ac	>100	44	>100
9n	>100	72	>100	9ad	>100	41	>100
9o	>100	27	>100	CA-4	NT@	< 0.1	NT
9p	>100	13	>100	ADR	< 0.1	< 0.1	< 0.1

*GI₅₀ value is considered to demonstrate highly significant activity at $\leq 1 \mu\text{M}$ (yellow highlighted), moderate activity at $\leq 10 \mu\text{M}$ (blue highlighted), low activity at $\leq 100 \mu\text{M}$ (green highlighted) and no activity ($>100 \mu\text{M}$) for synthetic compounds.

@ND: Not tested.

The data reflects GI₅₀ calculated from mean percent growth value at four different concentrations of three different experiments. Individual experiment was performed with each drug dilution in three replicates. Mean Growth percent data with standard error, along with individual three experiment percent growth values is provided in Supplementary Tables S1-S3.

CA-4: Combretastatin A-4 and **ADR: Adriamycin** employed as positive controls for SRB assay.

We had performed *in vitro* cytotoxicity studies for 10 cancer cell lines. However, it was observed from this data that these class of compounds are active mostly against oral cancer cell line, presumably in view of its selectivity towards this cell line.

Supplementary Figure S2 demonstrates growth curve profiles of SCC-29B oral cancer cells post treatment with phenstatin bearing indole linked chalcones (**9a-z** and **9aa-9ad**) for 48 hr. The comparative growth curve profiles of cancer cell lines HT-29 (colon), Hep-G2 (liver), and SCC-29B (oral) after treatment with compounds **9a**, **9f**, **9e**, **9l**, and **9b** are shown in Supplementary Figure S3. Cell growth response lines to compounds **Adriamycin** (Supplementary Figure S2), **9e**, and **9l** (Supplementary Figure S3) are flat and not descending, hence slope and intercept are not feasible for standard calculations. However, as we see, at 0.1 μ M cell growth was below 50%, hence we report GI50 as below 0.1 μ M. Only compound **9a** exhibited significant anti-proliferative activity against SCC-29B oral squamous cancer cells. Hence this compound was evaluated further for its anti-cancer efficacy in cancer stem-like cells (CSC) or spheroid assay and *in-vivo* NOD-SCID immunodeficient animal models.

2.2.2. Evaluation of anti-cancer potential using oral cancer spheroids

To evaluate the efficacy of compound **9a** to inhibit the growth of cancer stem-like cells, it was tested in a cytotoxicity assay using oral squamous cancer spheroids (SP) cells. Oral CSC were characterized by flow cytometry and were found to have increased populations of CD44⁺CD24^{lo} as compared to that found in an adherent SCC-29B cell line (Supplementary Figure S4, panels B and D). **ADR** drug uptake was also found to be significantly reduced in oral CSC as compared to adherent cell line (Supplementary Figure S4, Panel C). The drug uptake increased with time in the case of adherent as well as spheroid SP cells. Once characterized, both adherent oral cancer cell line and spheroid cells were tested against compound **9a** in the cytotoxicity assay. As evident in Figure 2A, compound **9a** affected the percent growth of oral cancer bulk (adherent) cells as well as cancer stem-like SP cells.

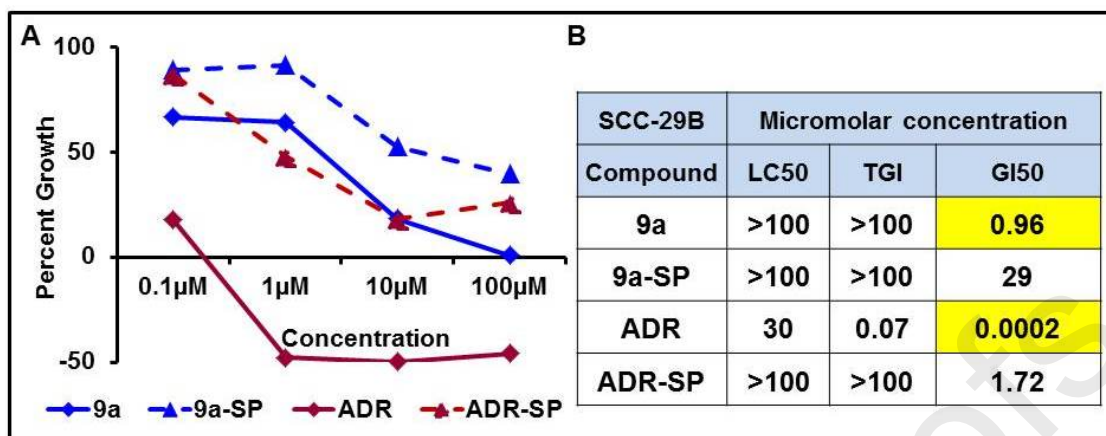


Figure 2: Chemosensitivity of compound 9a against oral cancer spheroids and adherent cells. SCC-29B cells were tested against **9a** and **Adriamycin (ADR)** in 48-hr SRB assay. Panel A exhibits line graphs for percent growth of SCC-29B adherent cells (intact line) and spheroids (SP, dashed line) for compound **9a** and **ADR**. This data is mean of three experiments. Standard error in each set was less than <3%. Spheroids cells exhibited reduced sensitivity to compounds compared to adherent counterparts. Panel B shows mean values of lethal concentration 50 (LC₅₀), total growth inhibition (TGI) and growth inhibition 50 (GI₅₀) of three experiments. It is evident that GI₅₀ value is higher for spheroids in comparison with that shown by adherent cells.

Oral CSC exhibited chemoresistance to compound **9a** as higher LC₅₀, TGI, and GI₅₀ concentrations (Figure 2) of **9a** were required for growth inhibition in comparison to that shown by their adherent counterparts (SCC-29B GI₅₀, CSC: 29 μM; adherent: 0.96 μM). Thus, the compound **9a** was found to be effective in growth inhibition against CSC as well as bulk oral cancer cells. The previous reports⁴⁸ showed that compounds which act on CSC besides non-CSC or bulk cells have better potential to reduce the tumor in xenograft study.

2.2.3. Evaluation of anti-tumor efficacy using an *in vivo* animal model

The *in vivo* antitumor property of this lead compound **9a** was further evaluated in the human xenograft carcinoma model employing adriamycin as a reference antitumor agent. The maximum tolerated dose (MTD) determination study for compound **9a** was carried out by studying acute toxicity. Compound **9a** when injected intravenous (i.v.) as one-time dose in NOD/SCID strain mice at 50 mg/kg and 25 mg/kg dose, exhibited very high toxicity with immediate mortality. Hence, the next dose of 12.5 mg/kg was tested i.v. as one time dose. At this dose, 50% of mice

died at the end of the 5 day period. It was observed that the compound was found to be well tolerated at 7.5 mg/kg dose by i.v. route (Supplementary Table S4). This study indicated that compound **9a** at 7.5 mg/kg (i.v. route) dose did not affect mice body weight significantly (Supplementary Figure S6). Therefore, 7.5 mg/Kg dose was considered as MTD for i.v. route (Supplementary Table S4). Based on these observations, for efficacy testing, the dosing protocols were designed as 2.5 mg/kg intravenously once a week for 4 weeks Mice per group n=6. The vehicle used for **adriamycin** was water. Vehicle used for **9a** dilution was DMSO for the first dilution and then water was used for further dilutions. Tumour volume, body weight, and signs of toxicity were monitored and recorded on respective days: 1, 5, 9, 12, 15, 18, 21, 24, 27, and 30.

It was interesting to note that the compound **9a** demonstrated substantial tumor reduction with respect to tumor-bearing control in a time-dependent manner (Table 2 and Figure 3). It was observed that compound **9a** via intravenous route exhibited better efficacy against AW13516 oral cancer xenograft (Figure 3). As evident from relative tumor volume and T/C ratio (Mean relative tumor volume for compound **9a** or standard drug **Adriamycin** treated groups over that of tumor-bearing control group on individual day data), compound **9a** exhibited a significant reduction in tumor volume by day 21 in i.v. dosing protocol and continued till the end of the study (percent regression 60%; T/C=0.4; Table 2 and Figure 3).

Table 2. Effect of compound 9a on tumor reduction of AW13516 oral cancer xenograft

Days	T/C Ratio*	
	ADR	9a
1	1.00	1.00
5	0.85	0.93
9	0.54	0.67
12	0.46	0.52
15	0.57	0.51
18	0.55	0.45

21	0.54	0.41
24	0.51	0.35
27	0.36[#]	0.44
30	0.32	0.40

*T/C ratio: Ratio of mean relative tumor volume for compound **9a** or standard drug Adriamycin treated groups over that of tumor bearing control group on an individual day. Mice per group n=6.

The vehicle used for adriamycin was water. The vehicle used for **9a** dilution was DMSO for the first dilution and then water was used for further dilutions.

Dosing protocols: **9a**, 2.5mg/kg once a week i.v. for 4 weeks; **Adriamycin**, 2.5mg/kg at day 1,5,9 i.v. i.v. intravenous; **ADR: Adriamycin**.

As per NCI guidelines, biological activity was considered as significant when T/C values were ≤ 0.42 (yellow highlighted and bold).

There was no significant body weight loss (Figure 3) and all experimental mice in treated groups survived till the end of the study. This indicated that compound **9a** did not exhibit toxicity for the provided dosing protocols and can be safely followed for further validation.

The tumor size seen in the animal groups was found to be concordant with the tumor volume recorded (Supplementary Figure S7 panel A). Median relative tumor volume for intravenous dosing protocol was found to be 4 cc for ADR-treated group and 2.32 cc for **9a** treated group as compared to 12 cc for tumor-bearing control (Supplementary Figure S7 panel B). Shrinking of oral cancer xenograft with compound **9a** treatment was found to have been initiated earlier than that shown by Adriamycin (Supplementary Figure S7 panel B).

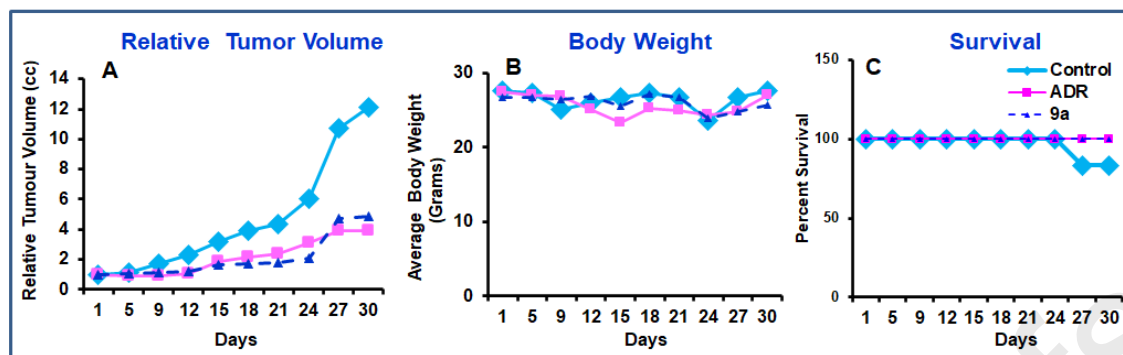


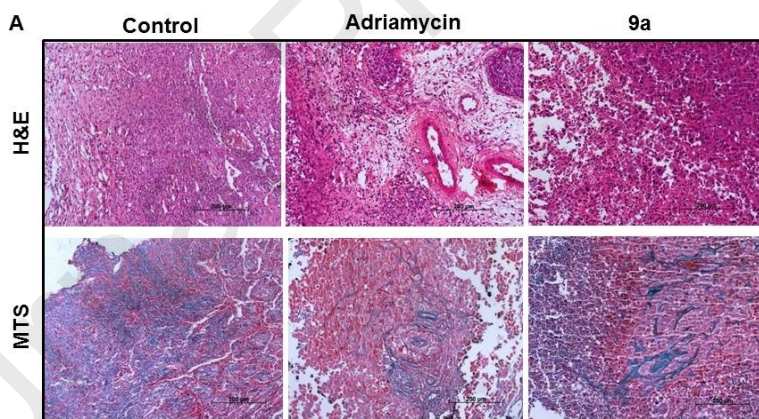
Figure 3: Effect of compound 9a on relative tumor volume, body weight and survival of experimental mice. The line graphs show (A) relative tumor volume (RTV), (B) mean body weight values in grams and (C) percent survival for treatment of AW13516 oral cancer xenograft bearing mice by an intravenous route at different time points in days for all groups studied. Figure legend in the rightmost panel depicts three groups in the study i.e. Control: tumor bearing control, **ADR**: Adriamycin treated and **9a**: **9a** treated mice group. Each group consisted of 6 mice. RTV was measured as tumour volume (TV) on the day of measurement/ tumour volume on day 1. RTV mean and Standard error (S.E.) values for each day are provided in Supplementary Table S5.

2.2.3.1. Histopathology studies

Xenograft tumors harvested at the end of the study at day 30 were processed for Hematoxylin & Eosin (H & E) staining. Microscopic images revealed that tumor-bearing control had increased angiogenesis and compact tissue architecture (Figure 4A). While the treated tumor sections demonstrated that angiogenesis was significantly reduced with increased necrosis. Masson-Trichrome stained (MTS) tumor sections showed increased collagen matrix (blue) in tumor-bearing control which got significantly reduced upon treatment with adriamycin and compound **9a** (Figure 4A).

Apgar et al (1998)⁴⁹ demonstrated that Masson's Trichrome stained sections can be better analyzed under fluorescence microscopy with higher sensitivity and recognition of special protein structures. They reported that red blood cells were stained bright red-orange, while cytoplasmic proteinaceous material was stained pale red.

Therefore in our study, MTS staining was followed to visualize cytoplasmic proteinaceous microtubule network distinctly in tumor tissue architecture before and after compound treatment. Tumor section stained by MTS were observed under laser confocal fluorescence microscope and it demonstrated that Adriamycin and compound **9a** were efficient in disrupting cytoskeleton components (stained pale red) as observed by cell body shrinkages, shortening of cell migratory processes and diffused microtubule protein staining; versus distinct microfilament staining and compact tissue architecture observed in tumor bearing control sections (Figure 4B and 4C). It was observed that bright red-stained red blood cells and fibrin components were also reduced in number after treatment with adriamycin and compound **9a** (Figure 4C). It was evident that in tumor sections of compound **9a**-treated animals, intercell adhesion was almost lost. Cell shape and integrity were also found to be greatly disrupted as compared to those observed in adriamycin-treated group tumor sections. This data clearly signifies the involvement of compound **9a** as microtubulin inhibitors.



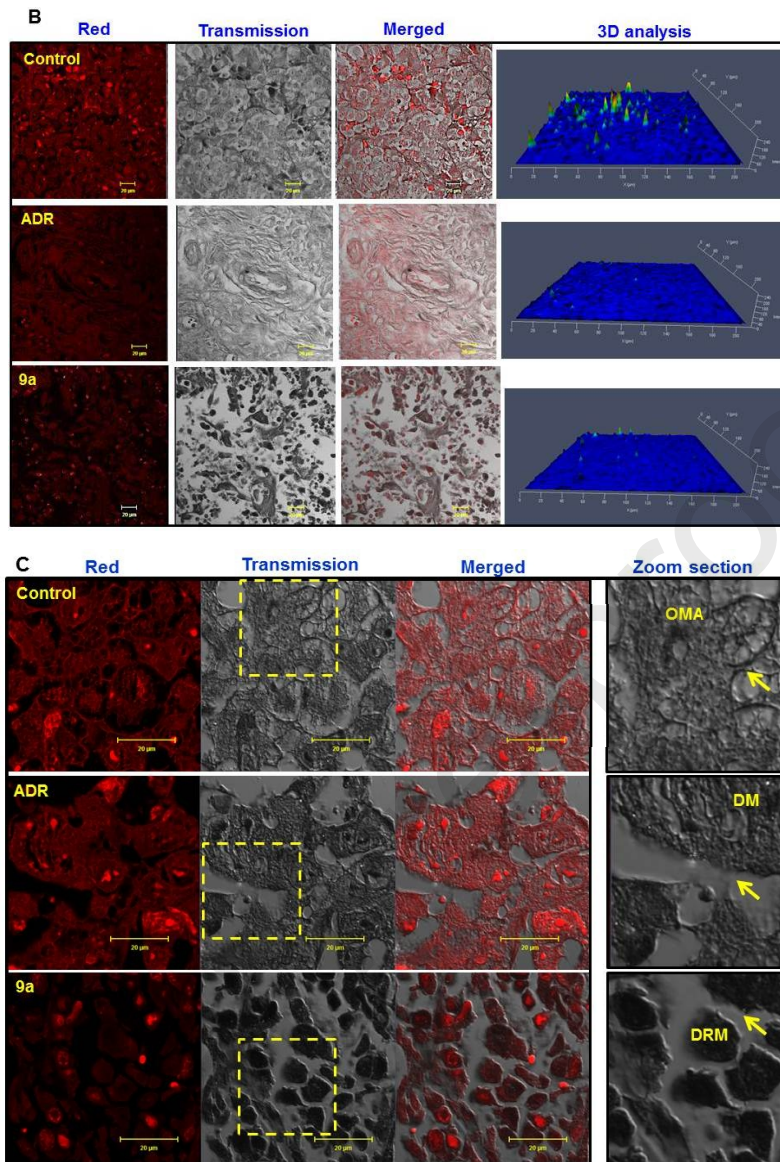


Figure 4: Histopathological changes in oral cancer xenograft tumors treated with 9a and Adriamycin. Panel A shows bright-field microscopic images of H & E stained (upper section) and Masson-Trichrome stained (MTS) (lower section) sections of oral cancer xenograft tumors from representative mice. Scale bar of 100 μm is shown at the right bottom of each image. Panel B and C shows MTS-stained laser confocal microscopic images of xenograft tumors along with a 3D plot of the signal intensity. Panel C shows magnified regions of representative sections from each animal experiment group. OMA-organized microtubule assembly; DM-disorganized microtubular structure and DRM-disorganized and reduced microtubular cytoskeletal proteins.

2.2.4. Effect of 9a on microtubule cytoskeleton of oral cancer cell line

Effect of **9a** on microtubule assembly of SCC-29B oral cancer cells was observed in an immunofluorescence assay. SCC-29B cells demonstrated normal cytoskeletal architecture with the presence of distinct Microtubule Organizing Centre (MTOC) near the nucleus (Figure 5A). Leading and trailing edges were clearly seen. Treatment with known tubulin destabilizer **CA-4** caused tubulin destabilization in these cells and tubulin was evident in amorphous form. Further, MTOC was lost in **CA-4** treated SCC-29B cells (Figure 5). It was interesting to note that the effect of **9a** on tubulin polymerization was confirmed as it caused destabilization of tubulin leading to the disorientation of microtubules, loss of MTOC, and cell integrity. Cells lost polygonal shape and got rounded due to loss of microtubule dynamics. **9a** at 2.5 μ M concentration also caused nuclear degradation and apoptotic blebbing (Figure 5A-a and Figure 5A-c). These observations were further confirmed at the ultrastructural level by transmission electron microscopy. Compound **9a** and positive control **CA-4** caused retractions and breakage of cell protrusions which are formed by microtubules and intermediate filaments^{50,51} (Figure 5B) Compound **9a** at concentration 5 μ M caused the complete destruction of tubulin architecture of SCC-29B cells (Data not shown).

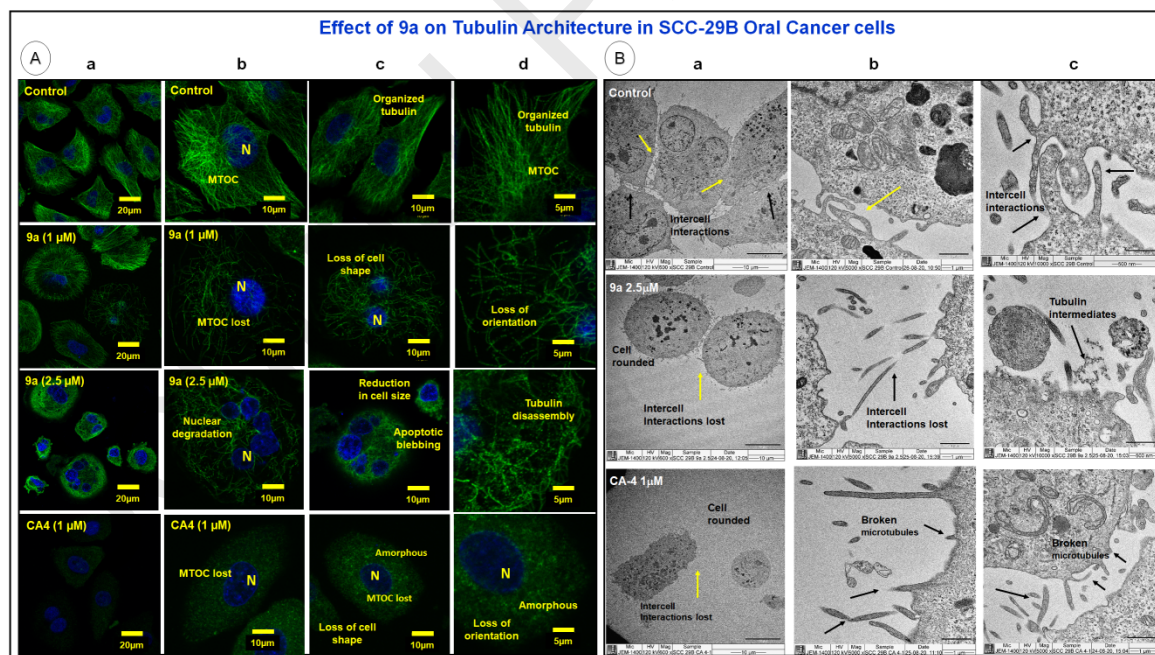


Figure 5: Effect of compound 9a on tubulin assembly in oral cancer cell line SCC-29B. SCC-29B cells were treated with compound **9a** (1 and 2.5 μ M) and known tubulin destabilizer **CA-4** (1 μ M) at

given concentrations for 24 hrs. Panel A depicts cell cultures treated with anti-tubulin antibody and observed by immunofluorescence assay. The control panel shows untreated cells with organized microtubules and intact polygonal cell shape. Treatment with **9a** caused the loss of tubulin polymerization leading to loss of cell integrity, reduction in cell size and induced apoptosis. Subpanels b, c, and d are magnified images. Scale bar is shown at the right bottom of each panel (a 20 μ m, b-c 10 μ m, and d 5 μ m). Panel B shows electron microscopy images of cultures treated with compound **9a** at 2.5 μ M and **CA-4** at 1 μ M. Arrows indicate intercellular tubular interactions that were found damaged after treatment with compounds. Subpanels b, and c are magnified images. Scale bar is shown at the right bottom of each micrograph (a 10 μ m, b 1 μ m, and c 500nm, 1 μ m).

2.3. Biophysical interaction of tubulin with compound **9a**

To evaluate the direct interaction of **9a** with tubulin and its effect on tubulin polymerization, *in vitro* polymerization assay and SPR assay were performed. **9a** demonstrated concentration-dependent increase in the inhibition of tubulin polymerization (Figure 6). **Paclitaxel** stabilized tubulin polymerization while **CA-4**, known tubulin assembly disruptor⁵², inhibited tubulin polymerization. This data was validated using transmission electron microscopy. At the ultrastructural level, tubulin filaments were found to be destabilized in presence of **9a** and **CA-4** (Figure 6C). **CA-4** at 5 μ M and **9a** at 10 μ M concentration exhibited typical microtubule intermediates and tubulin rings^{50,51}. Paclitaxel stabilized tubulin filaments (Figure 6C).

To further ascertain physical interaction between Tubulin and **9a**, SPR spectroscopic analysis was performed. Tubulin protein (0.13 μ M) was immobilized while the compound **9a** was present in the mobile phase. With an increasing concentration of **9a** ranging from 6.25 μ M to 100 μ M, a gradual increase in the association was observed in SPR response suggesting physical interaction between the two (Figure 6B). Compound CA-4⁵³ (well-characterized tubulin interactor) was used as a positive control to validate the interaction (Figure 6B). This result gave us evidence for the direct interaction of compound **9a** with tubulin.

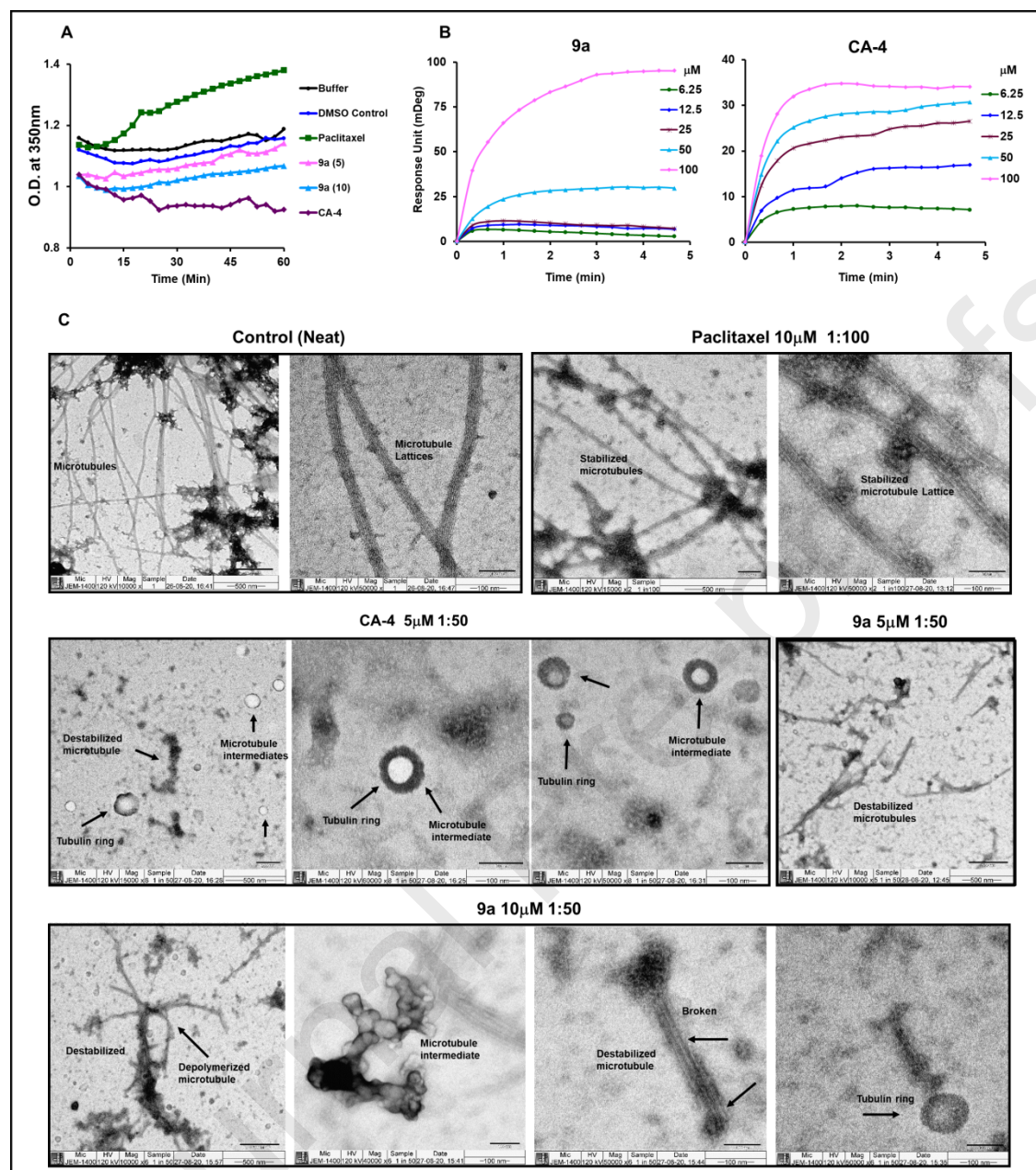


Figure 6: Effect of compound 9a on tubulin polymerization by direct physical interaction with tubulin in cell-free assays. A] *In vitro* tubulin polymerization kinetics assay. Tubulin in reaction buffer was incubated at 37°C in the buffer, vehicle control (DMSO at 0.0001%), compound **9a** (5 and 10 μ M), **Paclitaxel** (10 μ M) and **CA-4** (5 μ M). The tubulin assembly was quantitated by spectrophotometry. The experiments were performed twice, and representative data is shown. **B] Physical binding of 9a to tubulin by Surface Plasmon Resonance.** Panel B provides validation of the physical interaction of immobilized tubulin at different concentrations of the compound **9a** (present in the mobile phase). Compound **Combretastatin (CA-4, well-characterized tubulin interactor)** was used as a positive

control to validate the interaction with tubulin. An increase in response unit was observed with an increasing concentration of **9a** and **CA-4**. C] **Effect of 9a on cell-free tubulin polymerization at ultrastructure level by transmission electron microscopy.** Panel C shows electron micrographs after negative staining of tubulin treated with compounds for 90 min. Except for Buffer control (neat), other samples were diluted as neat samples had concentrated tubulin structures (**Paclitaxel** (1:100 dilution), **CA-4** and **9a** (1:50 dilution)). Scale bar is shown at the right bottom of each micrograph (500nm, 100nm).

2.4. Micro-PET-CT imaging

Tubulins and microtubules function as key modulators of mitochondrial metabolism. In particular, tubulins associate with enzymes of the glycolysis, preferential interactions between glycolytic enzymes and either the soluble or polymerized tubulin pool may also influence metabolic activity and microtubule dynamics.⁵⁰

Metabolic reprogramming especially glycolysis is one of the hallmarks of cancer. Cancer cells exhibit faster glucose consumption which can be visualized and monitored with [¹⁸F]-fluorodeoxyglucose (¹⁸F-FDG) positron emission tomography/computed tomography (PET/CT) scanning.⁴⁵ This method has broad applications in clinical oncology including diagnostics and monitoring therapy response. ¹⁸F-FDG uptake study was performed in tumor-bearing control and compound **9a** treated tumor mice at the end of the experiment at day 40 for evaluating the effect on tumor metabolism. It was observed that ¹⁸F-FDG uptake (Figure 7) was reduced by 75.8% in compound **9a** treated tumor (mean SUV 487 KBq/cc, Supplementary Videos S5 and S6) which was comparable to reduction of 68% as observed in adriamycin treated tumor (Mean SUV 644 KBq/cc, Supplementary Videos S3 and S4) over that shown by control tumor (mean SUV 2015 KBq/cc, Supplementary Videos S1, and S2).

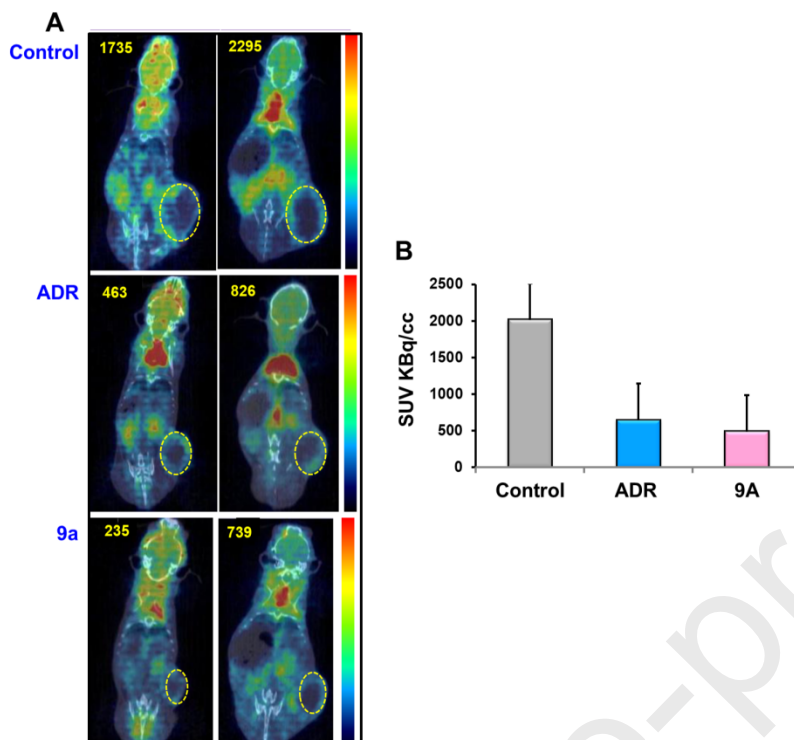


Figure 7: ^{18}F -FDG PET-CT imaging for metabolic changes in compound **9a**-treated AW13516 xenograft bearing mice. ^{18}F -FDG PET-CT exhibits the distribution of glucose uptake in tumor tissue. A] Immunodeficient oral cancer xenograft AW13516 bearing mice were imaged 4-hr after ^{18}F -FDG injection. Images shown are representative 2 mice from each group. Values on the top left of each panel exhibit the maximum standardized uptake values (SUVsKBq/cc) of tumors imaged at the end of the study (40 days). Yellow dotted circles mark the tumor boundary in individual mice. Glucose uptake was distinctly reduced in tumors from compound **9a**-treated mice as compared to control tumors. The color panel next to each group indicates uptake intensity from high (red) to low (blue). B] Bar graph depicts a quantitative analysis of maximum standardized uptake values (SUVsKBq/cc) of tumors imaged at the end of the study (tumor area marked with yellow dotted lines). Values represent mean \pm standard error of glucose uptake in two mice per group.

The vehicle used for adriamycin was water. The vehicle used for **9a** dilution was DMSO for the first dilution and then water was used for further dilutions.

Dosing protocols: **9a**, 2.5mg/kg once a week i.v. for 4 weeks; **Adriamycin**, 2.5mg/kg at day 1,5,9 i.v. i.v. intravenous; **ADR: Adriamycin**.

Glucose uptake relates to active proliferation in xenograft tumor tissues. Further, Vergez et al⁵⁴ reported that ¹⁸F-FDG PET-CT imaging provided an early indication of head and neck squamous cancer xenograft treatment which was well correlated with clinical outcome in a human clinical trial. Thus, a significant decrease in glucose uptake indicated that compound **9a** successfully abrogated proliferation and glycolysis metabolism of tumor cells in oral cancer xenograft in an animal model which may have immense potential as well in human clinical trials.

2.5. Molecular docking studies

The studies suggest that these synthesized compounds exert their effect by acting as microtubule inhibitors. For better understanding and to know how these phenstatin based indole linked chalcone compounds interact with tubulin, the potential binding modes for two of the most potent compounds, **9a** and **9e**, were investigated at the colchicine binding site in the tubulin dimer, the colchicines bind at the interface of α β -tubulin subunits, both the chains were considered for molecular docking studies. The tubulin crystal structures were obtained from Protein Data Bank (PDB ID code: 3UT5).⁵⁵ The protein preparation was done using the Schrodinger's tool (PPrep). Both **9a** and **9e** were sketched by using 2D Sketcher and Schrödinger's LigPrep program was used to generate different conformations of ligands. Molecular docking studies were performed using a GLIDE docking module of Schrödinger suite and the results were analyzed on the basis of the GLIDE docking score and molecular recognition interactions. The 3D figures were obtained using Schrödinger Suite 2017-1.⁵⁶

Figure 8 illustrated the overview of the potential binding site of compounds **9a** and **9e**, which binds at the interface of α - and β -tubulin. Molecular docking results along with hydrogen bonding as well as hydrophobic results for compound **9a**, **9e** with tubulin protein was depicted in Supplementary Table S6. According to previous studies, the Asn α 101 could also play a role as strong hydrogen bond donors. The binding modes with the active site were observed to be very similar to previous results as reported for colchicine and various other colchicine binding site inhibitors.⁵⁷ Figures 8A and 8B showed that the trimethoxy rings of both compounds **9a** and **9e** were well-positioned in proximity to the Lys β 254, Gln α 183 and Ala180 residues, and they adopt an orientation very similar to that of the trimethoxy ring of colchicine in the crystallized

structure. The interaction was strongly stabilized by hydrogen bonds. Hydrogen bonding interactions of compounds **9a** and **9e** include C=O of trimethoxybenzoyl moiety with ASN α 101 at distance of 1.85 Å and C=O of chalcone with Ser α 178 at distance of 2.19 Å, similar to that compound **9e** formed with ASN α 101 at a distance of 2.18 Å and with Ser α 178 at distance of 2.10 Å. In addition, compound **9e** has formed one more hydrogen bond between methoxy of trimethoxybenzoyl moiety and Tyr α 224 at distance of 2.04 Å. Whereas, compound **9a** highlighting the pi-cation interaction with Lys β 254 at the colchicine binding site. Moreover, compounds **9a** (turquoise) and **9e** (grey) overlapped well with the native ligand colchicine (green) in Supplementary Figure S8 and bind at the colchicine binding site. The indole ring occupied the site where the 7-membered ring in colchicine binds, while the 3,4,5-trimethoxybenzoyl group of compounds **9a** and **9e** overlapped very well with the 3,4,5-trimethoxyphenyl ring in colchicine. Most interactions of compounds **9a** and **9e** were driven mainly by hydrophobic interactions with Gln11, Thr179, Ala180, Gln183, Arg221 and Tyr224, amino acids of the α -tubulin and Cys241, Leu248, Lys254, Leu255, Asn258, Met259, Val315, Ala316, Ile318, Met325 and Lys 352 amino acids of the β -tubulin.

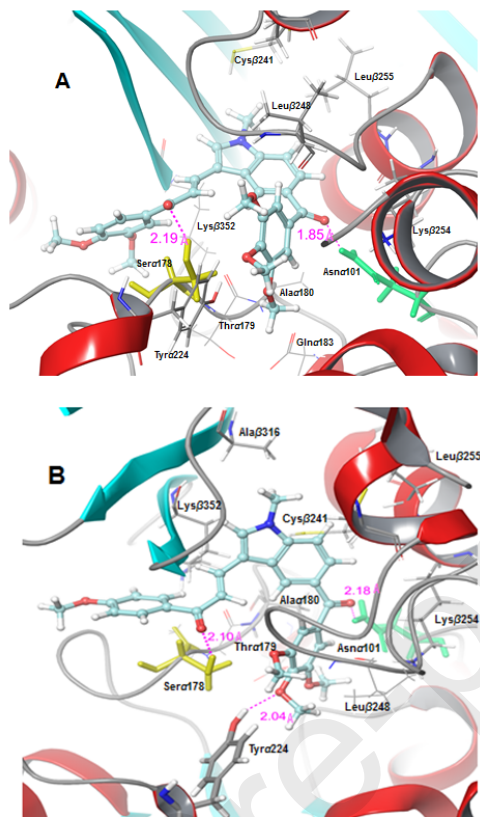


Figure 8. Proposed binding mode of (A) compound **9a** (turquoise) and (B) compound **9e** (turquoise) in the colchicine binding site of tubulin (PDB ID code: 3UT5) shown as a ball and stick. Interacting residues of α - and β -tubulin are presented as tube and wire. Hydrogen bonds are represented with pink dotted lines (in Å). Images were generated using Maestro, Schrodinger, LLC.

The validation of docking was conducted by redocking of the bound ligand colchicine in the colchicine binding site of tubulin protein. The bound and docked conformations of colchicine showed similar interactions and binding pose at the binding site with a root mean square deviation (RMSD) of 1.7230 Å (Supplementary Figure S9).

The bioenergetic and biosynthetic pathways are primarily altered in cancer. Recently efforts are being focused to identify inhibitors that are capable of affecting multiple enzymes simultaneously in tumor metabolism pathways.⁴⁶ Since we observed a significant effect of **9a** on glucose uptake in an oral cancer xenograft model, we analyzed **9a** for its effect on a series of enzymes in the glycolytic pathway and TCA cycle.

The crystal structures of some of the key metabolic regulatory enzymes described by Yadav et al.⁴⁶ i.e. GAPDH (PDB ID: 1U8F)⁵⁸, HK 2 (PDB ID: 2NZZ)⁵⁹, LDH (PDB ID: 1I0Z)⁶⁰, PGK (PDB ID: 4AXX)⁶¹, PDH (PDB ID: 3EXE)⁶² and IDH1 (PDB ID: 4UMX)⁶³ were obtained from RCSB-Protein Data Bank. The grid box was generated around the active site residues present in the receptors.⁵⁷ Finally, the 3D structure of compound **9a** was docked into the active sites of GAPDH, HK 2, LDH, PGK, PDH and IDH1 enzymes using Schrödinger Suite 2017-1.⁵⁵ We observed that the resolution of crystal structures of enzymes of the glycolytic pathway and TCA cycle was found to be in the range of 1.5-2.5 Å, which is considered optimal for docking. Hence crystal structures of these PDBs were considered for our modelling work.

Supplementary Table S7 demonstrates the result of the molecular docking along with hydrogen bonding as well as arene-arene interactions of compound **9a** with the different metabolic regulatory enzymes. Thus, these molecular docking data provided a detailed account of interactions of compound **9a** with that of targeted receptors. Compound **9a** exhibited good binding properties with the key metabolic regulatory enzymes and these studies intended for some important directions for future structural modifications.

Rai et al.⁶⁴ have observed that inhibitors of LDH, a key glycolytic enzyme that catalyzes the final step in the glycolytic pathway, significantly affected the growth of pancreatic cancer cell line Mia-Pa-Ca-2 and sarcoma cell line A673 *in vitro* cytotoxicity assay. They also predicted robust cell-based inhibition of target. Hence reduced glucose uptake observed in our PET-CT imaging study, after treatment of xenograft with **9a** can be justified that it must be through inhibition of target metabolic enzymes of the glycolytic pathway and TCA cycle.

Overall, these molecular docking results gave us a detailed explanation of interactions of compound **9a** with colchicine binding site of tubulin and also key metabolic regulatory enzymes of glycolysis pathway.

3. CONCLUSION:

In conclusion, we have synthesized a series (**9a-z** and **9aa-ad**) of phenstatin bearing indole linked chalcones and evaluated them for their antiproliferative activity on few cancer cell lines.

Compound **9a** demonstrated significant anti-proliferative activity against oral cancer squamous cancer cells as well as oral cancer stem-like spheroids. It was further tested in oral cancer xenograft AW13516 in an immunodeficient mouse model. It was efficacious in significantly reducing tumor volume without causing any toxicity in experimental mice. Interestingly, it also reduced angiogenesis in mice xenografts, reduced collagen levels and caused significant reduction in cell processes, cellular integrity as well as cytoskeletal organization. Moreover, it successfully abrogated glucose uptake in tumor xenografts. *In vitro* tubulin polymerization kinetics assay revealed direct interaction of **9a** with tubulin and inhibition of tubulin polymerization leading to destabilization, protofilament bending and generation of tubulin ring intermediates. SPR assay further confirmed the physical binding of **9a** with tubulin. *In silico* molecular docking of **9a** to the colchicine binding site of tubulin and metabolic enzymes of glycolysis/ TCA cycle, demonstrated a better binding affinity to target binding site and consequently inhibition of microtubule polymerization and glucose metabolism. Based on these *in silico* and pre-clinical observations, compound **9a** consisting of phenstatin based indole-chalcone scaffolds can be considered as an attractive tubulin polymerization inhibitor candidate for developing anti-cancer therapeutics. Further investigations on safety and acute/ chronic toxicity of compound **9a** are warranted to proceed under the drug-development pipeline.

4. EXPERIMENTAL SECTION:

4.1. Chemistry

All solvents and reagents were purchased from commercial sources and were used without further purification. Reactions progress was routinely monitored by TLC on silica gel glass plate containing 60 GF-254, and compounds visualized with UV light, iodine vapor and H₂SO₄. ¹H and ¹³C NMR spectra were recorded on Bruker UXNMR/XWIN-NMR (300 MHz) or InnovaVarian-VXR-Unity (400, 500 MHz) instruments. Chemical shifts (δ) were reported in parts per million (ppm) downfield from TMS expressed as internal standard and coupling constants are expressed in Hz. ¹H NMR spectral data were reported in the following order: multiplicity (s, singlet; brs, broad singlet; d, doublet; dd, doublet of doublets; t, triplet; m,

multiplet), coupling constants in Hz, and a number of protons. ESI mass spectra were recorded on Micromass Quattro LC (ESI+ software with capillary voltage 3.98 kV and positive ion trap detector). QSTAR XL Hybrid MS-MS mass spectrometer was used to record High-resolution mass spectra. Melting points were determined with an electrothermal digital melting point apparatus IA9100 and are uncorrected. The purity of the compounds was determined by HPLC performed on a Shimadzu LC-20AD apparatus equipped with a SPD-M20A diode array detector and a Shimadzu SIL-20AC auto-injector using C18 column (waters 5 μ M C18, 4.6 mm 250 mm column). Elution conditions: mobile phase A (85%)-acetonitrile; mobile phase B(15%)-water, pH 4.3 adjusted with 0.1% formic acid + 10 mM NH_4OAc . The flow rate was 1.0 mL/min and the injection volume was 5 μ L at 25 $^\circ\text{C}$ and detection at 254 nm.

4.1.1. General procedure for the synthesis of compounds (11a–c)

To a stirred solution of 5-bromo-1*H*-indole (1 mmol) in dry THF, was added NaH (1.5 equiv, 60% dispersion in mineral oil) portion wise at 0 $^\circ\text{C}$ and stirring was continued at room temperature for 30 min. Then, methyl iodide/ethyl bromide/*tert*-butyldimethylsilyl chloride (1.2 equiv) were added at 0 $^\circ\text{C}$ and the reaction mixture was allowed to warm to room temperature with continuous stirring for 3 h. Then ice cold water was added carefully and extracted using CH_2Cl_2 . The combined organic extracts were washed with water and saturated brine solution, dried over Na_2SO_4 and concentrated under vacuum. Then the obtained crude mixture was purified by column chromatography using ethyl acetate and petroleum ether as an eluent to give pure compounds **11a-c**.

4.1.2. General reaction procedure for the synthesis of compounds (12a-c)

To a solution of the above compounds (**11a-c**, 1 equiv) in dry THF, *n*-BuLi (1.2 mmol, 1.6 M in hexane) was added at -78 $^\circ\text{C}$ under argon atmosphere and stirred for 1 h. Then 3,4,5-trimethoxybenzaldehyde (1 equiv) was added slowly to the reaction mixture and the reaction mixture was allowed slowly to reach the room temperature and stirred for 4 h. Then reaction mixture was poured into ice-cold water and extracted with CH_2Cl_2 , washed with water and saturated brine solution. Then the combined organic layer was dried over Na_2SO_4 and concentrated under vacuum. The resulted residue was purified by column chromatography using ethyl acetate and petroleum ether as an eluent over silica gel to give pure compounds **12a-c**.

4.1.3. General reaction procedure for the synthesis of compounds (13a-c)

To a stirred solution of compounds (**12a-c**, 1 equiv) in DMSO, IBX (2 equiv) was added at 0°C and stirred at room temperature for 3 h. After completion of the reaction, monitored by using TLC the reaction mixture was poured into ice water and extracted with CH₂Cl₂, the combined organic extracts were washed with water and saturated brine solution. The combined organic extracts were dried over Na₂SO₄ and concentrated under vacuum. The obtained crude was purified by column chromatography using ethyl acetate and petroleum ether as an eluent over silica gel to afford pure compounds **13a-c**.

4.1.4. General reaction procedure for the synthesis of compounds (14a-c)

To a stirred solution of DMF (2.5 equiv) in CHCl₃ (5 mL) was added POCl₃ (2 equiv) dropwise at 0 °C for preparing Vilsmeier reagent. To this reagent, compound **13a-c** (1 equiv) dissolved in CHCl₃ (60 mL) was added dropwise, the reaction mixture was warmed to 27 °C and stirred for 2 h, then refluxed for 12 h. The solvent was removed under vacuum. After completion of the reaction, the reaction mixture was poured onto ice and neutralized by saturated sodium bicarbonate solution. The resulting crude solid was filtered and recrystallized using ethanol to obtain aldehydes **14a-c** in high purity.

4.1.5. General reaction procedure for the synthesis of compounds (9a-9z and 9aa-9ad)

To a solution of aldehydes **14a-c** (1 equiv) in ethanol, substituted acetophenone (1 equiv) and 10% aqueous sodium hydroxide (3 mL/100mg) were added and the reaction mixture was stirred for 6 h at room temperature. After completion of the reaction monitored by TLC, the solvent was evaporated under vacuum. The resulted crude product was dissolved in ethyl acetate and washed with water and brine solution. The organic extract was dried over Na₂SO₄ and concentrated in vacuo. The residue was finally purified by column chromatography using ethyl acetate and petroleum as a solvent system over silica gel to obtain the pure product.

4.1.6. (*E*)-1-(3,4-dimethoxyphenyl)-3-(1-methyl-5-(3,4,5-trimethoxybenzoyl)-1*H*-indol-3-yl)prop-2-en-1-one (**9a**)

The compound was synthesized according to the general procedure using **14a** (100 mg, 0.28 mmol), acetophenone (51 mg, 0.28 mmol) and 10% aqueous sodium hydroxide solution (3 ml) to obtain pure product **9a** as a pale yellow solid. Yield: 133 mg (78%); mp: 239-241 °C. ¹H NMR

(500 MHz, CDCl₃) δ 8.56 (s, 1H), 8.04 (d, J = 15.5 Hz, 1H), 7.79 (s, 1H), 7.65 (d, J = 1.9 Hz, 1H), 7.62 (d, J = 15.5 Hz, 1H), 7.55 (s, 1H), 7.49 (d, J = 5.6 Hz, 1H), 7.47 (d, J = 5.6 Hz, 1H), 7.14 (s, 2H), 7.01 (d, J = 8.4 Hz, 1H), 3.96 (d, J = 5.5 Hz, 9H), 3.88 (s, 9H); ¹³C NMR (101 MHz, CDCl₃) δ 195.92, 195.69, 153.07, 152.91, 152.88, 149.24, 141.56, 140.21, 139.86, 135.39, 132.64, 130.92, 126.03, 125.50, 124.90, 122.61, 117.74, 114.52, 110.06, 107.96, 107.61, 61.02, 56.34, 56.31, 33.97; ESI-MS: m/z 516 (M + H)⁺; HRMS (ESI) m/z for C₃₀H₃₀O₇N calculated m/z : 516.2017, found m/z : 516.2005; HPLC: t_R 5.63 min, purity 97.4%.

The characterization data for intermediates and other 9-series compounds including HPLC data is provided in the supporting file.

4.2. Biology

4.2.1. *In vitro* cytotoxicity of compounds by SRB assay

4.2.1.1. Cell culture

Cancer cell line HT-29 (colon) was procured from NCI, USA; SCC-29B (oral) was provided by Dr Susanne M. Gollin, University of Pittsburgh, Pennsylvania, USA; and Hep-G2 (liver) was procured from NCCS, Pune. All the cell lines were maintained in RPMI or DMEM medium (Life Technologies, USA) in presence of 10% fetal calf serum, 2 mM L-glutamine and 1% antibiotics.

4.2.1.2. SRB assay

In vitro cytotoxicity, SRB assay was performed as described previously.^{65,66} SRB assay is a rapid, sensitive, cost-effective and high-throughput method used for the quantification of cellular proteins and forms an integral part of *in vitro* drug screening in the Developmental Therapeutic Program of the National Cancer Institute (NCI), USA. For this assay, the cells were dispensed at a density of 5000 cells/ well/ 100 μ L in 96-well flat-bottom microtiter plates (Eppendorf Inc, USA). Cells were allowed to adhere by incubating plates at 37 °C in 95% humidified air with 5 % CO₂ for 24 h. Compounds **9a-9z** and **9aa-9ad** were dissolved in dimethyl sulfoxide (DMSO) and further diluted with a plain medium. Compounds were added to cells in triplicates at final concentrations of 0.1, 1, 10 and 100 μ M and plates were further incubated for 48 hours in 37 °C incubator. Only cells served as cell control, while wells with the addition of **Adriamycin (ADR)**

served as a positive control. Each experiment was performed three times. At the end of 48 hours of incubation, morphological changes in cell cultures were observed and cells treated at the highest drug concentration were captured using Phase Contrast Inverted Microscope (Model Eclipse Ti-S, NIKON Co., Japan) fitted with the digital camera to the computer. Further, the cell proteins were fixed using 10% trichloroacetic acid. Proteins were stained with SRB dye and bound stain in the cell proteins was subsequently eluted with 10mM Trizma base. The absorbance was read on a plate reader (Model Sunrise, Tecan Inc., USA), at a wavelength of 540 nm with a 690 nm reference wavelength. Percent growth was calculated set wise and was expressed as the ratio of average absorbance (O.D.) of the test well to the average absorbance of the control wells.

$$\text{Percentage of control cell growth} = \frac{\text{Mean OD sample at 48hr} - \text{Mean OD 0 hr}}{\text{Mean OD cell control at 48hr} - \text{Mean OD 0 hr}} \times 100$$

The following values which implicates the cytotoxicity of each drug on each cell line, namely LC₅₀ (Concentration of drug causing 50% cell kill), GI₅₀ (Concentration of drug causing 50% inhibition of cell growth) and TGI (Concentration of drug causing total inhibition of cell growth) were calculated. GI₅₀ value of $\leq 1\mu\text{M}$ was considered to demonstrate activity in case of synthetic compounds.

4.2.2. Oral cancer spheroid cell culture (CSC) assay

It was observed that spheroid cultures consisting of cancer-stem-like cells exhibit increased drug resistance or less chemosensitivity as compared to their adherent cell counterparts.⁶⁷ To determine if compounds that showed activity against bulk cancer cells have any growth inhibition efficacy against stem-like cells of oral cancer, compounds were tested against oral cancer spheroids in CCK-8 dye assay. Oral cancer cell line SCC-29B cells were dispensed at a seeding density of 5000 per well in matrigel coated 96-well Flat bottom plates (Eppendorf India Ltd). MEM serum-free medium reconstituted with 1% B27 supplement, 20 ng/ml of Epidermal Growth factor and 20 ng/ml of Basic Fibroblast Growth Factor (Life Technologies, USA) was added every 48 hr and repeated for two cycles. Sphere-like structures were visible after 6 days. Spheroids were characterized for a stem-like population by flow cytometry for CD44⁺ CD24^{lo}

CSC and reduction in dye uptake. For *in vitro* chemosensitivity assay, compound **9a** and standard anti-cancer drug **Adriamycin** were added at various concentrations 1, 1, 10 and 100 μM to the wells and spheroids were further incubated for 48 hr at 37 °C incubator with humidified atmosphere and 5% CO_2 in air. Images were captured under a phase-contrast inverted microscope (Model Ti-S, Nikon Instruments) at 20 \times magnification. Comparative cell culture assay was also set up using SCC-29B adherent cell culture. Experiments were repeated thrice for statistical evaluation and each experiment was set up in triplicate wells. At the end of assay 10% CCK-8 dye (Dojindo Molecular Technologies, Inc., Japan) was added to each well and after 3 hr of incubation, plates were read in an ELISA reader (Model Sunrise, TecanInc., Switzerland) at 450 nm with a reference wavelength of 595 nm. Percent growth for each spheroid set was calculated based on control cultures and data was represented as GI_{50} in micromolar concentrations.

4.2.3. *In vivo* efficacy of compound 9a using oral cancer xenograft in an immunodeficient mice model:

To evaluate *in vivo* efficacy of compound 9a, oral cancer xenograft AW13516 was selected. Oral cancer cell line AW13516 was used to develop xenograft in an immunodeficient NOD-SCID mouse model. All procedures involving mice were performed according to protocols approved by Institutional Animal Ethics Committee, ACTREC, Tata Memorial Centre, Navi Mumbai (Proposal # 1/2015) and were adhered to CPCSEA guidelines (Registration Number: 65/GO/ReBiBt/S/99/CPCSEA). Six to eight week-old in house bred male NOD-SCID mice were housed in micro-isolator cages on vented racks and handled under laminar flow hoods fitted with HEPA filters. Animals received human care and all efforts were undertaken to minimize animal suffering before and during experiments.

4.2.3.1. Acute toxicity studies for compound 9a

Acute toxicity for compound **9a** was determined using immunodeficient NOD-SCID mice by intravenous (i.v.) route. Six animals were employed for each dose tested. Mortality and weight loss ≥ 4 grams/ mouse were considered to indicate toxicity criteria.⁶⁸ Different doses of the compound **9a** ranging from 20-100mg/kg body weight were injected as one time dose (i.p or i.v.)

into mice and mice were monitored for any physical signs of toxicity or mortality till day 5 post-dosing.

4.2.3.2. Efficacy experiment design

Anti-cancer efficacy of **9a** was evaluated as per the modified method of previously reported *in vivo* assay⁶⁹. The cryopreserved AW31516 oral cancer tumor was passaged to obtain donor mice. For induction of tumour, small pieces of ~4-5 mm of AW31516 xenografts were subcutaneously implanted on to the flank region of male NOD-SCID mice. When average tumor volume reached approx. 50 to 60 mm³, all the mice were randomized into desired groups (n=6/group) before the start of the treatment. The groups consisted of tumor bearing control (Group A), Adriamycin-treated (i.v.) group as positive control (Group B), compound **9a** treated (i.v.) group (Group C). The vehicle used for adriamycin was water. The vehicle used for **9a** dilution was DMSO for the first dilution and then water was used for further dilutions. Dosing protocol for **9a** treatment was 2.5mg/kg once a week i.v. for 4 weeks and for **Adriamycin** it was 2.5mg/kg at day 1,5,9 i.v. Tumor measurements were carried out to determine tumor growth and tumor volume using a digital Vernier caliper (Pro-Max, Electronic Digital Caliper, Fowler-NSK, USA). Mice were observed at regular intervals for period of around 30 days for body weight, tumor volume and mortality. The data was represented as Relative Tumor Volume (RTV in cc), T/C (ratio of test versus control) and survival. Tumor volume was calculated using formula $[(w1 \times w1 \times w2) \times (\pi/6)]$, where w1 and w2 were the smallest and the largest tumor diameter (cm), respectively. RTV was measured as tumour volume (TV) on day of measurement/ tumour volume on day 1. The T/C ratio is an indication of antitumor effectiveness. The percentage treatment/control (T/C%) values or percent tumor regression values were calculated as follows:

Relative Tumor Volume (RTV): TV on day of measurement/ TV on day 1

T/C ratio= RTV_Test/ RTV_Control

Tumor Regression %= 100-[T/C*100]

T = mean tumor volume of the drug-treated group; RTV = mean tumor volume of the drug-treated group on the study day of interest – mean tumor volume of the drug-treated group on initial day of dosing; C = mean tumor volume of the control group. As per NCI, USA guidelines,^{70,71} biological activity was considered as significant when T/C values were ≤ 0.42 .

The percentage of survival was calculated at the end of the study for each animal and each

compound was administered. On the day of sacrifice, tumor pieces were preserved in 10% formalin for histopathology.

4.2.3.3. Micro-PET imaging studies

At the end of the study on day 40, two animals from each group were processed for the imaging experiment. The animals were anaesthetized by inhalation of isoflurane/oxygen mixture [3% isoflurane/97% oxygen (v/v)] at a flow rate of 1L/ min for 2-3 min. About 200 μ L (~22 MBq/600 μ Ci) of 18 F-FDG was then administered intravenously via the tail vein. After 1 h, the animal was again anaesthetized following the above inhalation mixture and anaesthetic effect was maintained by isoflurane/oxygen mixture [2% isoflurane/98% oxygen (v/v)]. The animal was appropriately positioned in the PET scanner and whole-body images were acquired for 20 min using micro PET/SPECT/CT tri-modality gamma imaging system (Triumph, Gamma Medica Ideas, Northridge, CA, USA). The animals were kept fasting overnight before 18 F-FDG administration. Whole body CT images (magnification 1.3, FOV 91.08, energy 40 KeV, 600 ms and 512 projections) of the animal were subsequently acquired without disturbing the position of the animal. The animals were restrained at a position over the detector under continuous gaseous isoflurane anesthesia. The data was viewed and analyzed in PMOD data analysis and quantitation software v3.9 (PMOD Technologies, Ltd, Zurich, Switzerland). The uptake of the tracer in the tumor was obtained by measuring the standard uptake value (SUV) drawing ROI over the uptake in tumor. Three dimensional videos were made using advanced volume rendering and data visualization software VIVID 3D based on Amira 4.1 platform designed for Gamma Medica-Ideas.

4.2.3.4. Histopathology studies

Formalin fixed tumor samples were processed in paraffin wax for histopathology studies. Tissue blocks were trimmed using an ultramicrotome to obtain sections of 4-6 μ m. Tissue sections were dried and stained with Hematoxylin & Eosin dye. Changes in tissue architecture in control versus treated tumors were recorded under a bright light microscope (Carl Zeiss Microscope, Zeiss Inc., Germany).

4.2.3.5. Masson's Trichrome staining

Tissue sections were stained with standard Masson's Trichrome staining protocol provided in the Armed Forces Institute of Pathology Staining Manual⁶⁷ and changes in tissue architecture in control versus treated tumors were recorded using bright light upright microscope (Carl Zeiss Microscope) as well Laser Confocal microscope (LSM 780 model, Zeiss Inc., Germany). Images were analyzed using Zen Software (Carl Zeiss Inc, Germany).

4.2.4. Effect on tubulin assembly in SCC-29B cells

To evaluate the effect of **9a** on microtubule structure, SCC-29B oral cancer cells were treated for 24 hours at 37°C in the presence or absence of **9a** at 1, 2.5 and 5 µM. **CA-4** was used at 1µM as a positive control. Untreated and treated SCC-29B cells were fixed with 4% paraformaldehyde for 30 min and then treated with mouse anti-human tubulin antibody (Sigma Aldrich, Merck, USA) for 2hrs at room temperature. Secondary antibody goat anti-mouse tagged with fluorescein isothiocyanate (FITC) was used for the detection of microtubule architecture inside cells for 1 hr at room temperature. Cells were counterstained with DAPI for localization of the nucleus. The experiment was conducted thrice for reproducibility. Stained cells were acquired on a Confocal microscope (LSM 780 model, Zeiss Inc., Germany). Images were analyzed using Zen software (Carl Zeiss Inc, Germany).

SCC-29B cells treated for 24 hrs with compound **9a** (1 and 2.5 µM) and known tubulin destabilizer **CA-4** (1 µM) were also analyzed for changes in tubulin assembly at the ultrastructural level. Cells before and after treatment were fixed in 5% glutaraldehyde for electron microscopic analysis and processed as mentioned previously⁶⁹. Images were captured using a Transmission Electron Microscope (Jeol 1400 Plus, Jeol, Japan) with a digital camera and analysed (iTEM Analysis Software, Olympus).

4.3. Biophysical interaction studies

4.3.1. *In vitro* Tubulin Polymerization Kinetics Assay:

The effect of compound **9a** on tubulin polymerization kinetics was evaluated as per the method described previously⁵². In brief, pure bovine tubulin (≥99%, Sigma-Aldrich, Merck, USA) was prepared as per the manufacturer's instructions and added to wells on a 96-well plate containing the different concentrations of test compounds. Buffer and DMSO (0.001%) served as a negative

control. **Paclitaxel** at 10 μ M served as polymerization and tubulin stabilization control. Known tubulin destabilizer **CA-4** at 5 μ M served as positive tubulin polymerization inhibition control. Compound **9a** was tested at 5 and 10 μ M concentrations. Samples were mixed well, and tubulin assembly was monitored every 2.5 min intervals for 60 min at 37°C (mild shaking for continuous mixing) at optical density (O.D.) 350nm in a Microplate Spectrophotometer (Epoch™ 2, BioTek Instruments, Inc., Winooski, VT, USA). Kinetics data were recorded using equipment-associated reader version 2.09.1. The experiment was repeated twice for evaluating reproducibility.

After 90min of tubulin interaction, ten μ l aliquots from each test and control samples were applied onto the grid and after 10 minutes drained off excess sample using filter paper from the edge of the grid. Then immediately stained the grid by applying 10 μ l of 1% uranyl acetate (Ted Pella Inc, USA) for 1 minute and then drained off excess uranyl acetate. After air drying, the grid was viewed under Transmission Electron Microscope (Jeol 1400 plus, JEOL, Ltd, Akashima, Japan) at 120 KV and micrographs were captured using CCD bottom-mount camera (Model Tengra, Münster, Germany).

4.3.2. Surface Plasmon Resonance:

To understand the interaction between Tubulin and compound **9a** (515.55 Da), SPR (Autolab Esprit, Netherland) was performed. Bare gold sensor chip was used employing EDC-NHS chemistry (Autolab ESPIRIT SPR User manual) to assess the interaction as described earlier.⁷² At 20°C, about 750 response units of Tubulin (GST-tagged human recombinant protein, Sigma Aldrich Merck, USA) were loaded onto chip followed by extensive washing with buffer [50 mM Tris (pH 7.5)]. Different concentrations (6.25 μ M–100 μ M) of the **9a** molecule and control **CA-4** (334.4 Da) were injected onto the Tubulin-bound sensor chip. The small molecule was allowed to interact with the immobilized tubulin for 300 s before washing off with buffer. The data were processed using the Autolab kinetic evaluation software (V5.4) provided with the instrument.

4.4. Statistical analysis

Data were expressed as the mean of three independent experiments in the *in vitro* cytotoxicity assays. The data was analyzed by the mean graph technique described by Holbeck et al⁷¹ to investigate the effect of individual compounds on each cancer cell line. For *in vivo* experiments, results were expressed as Mean \pm Standard error. For comparing more than two groups in *in-vivo* study, the parametric analysis of variance (ANOVA) was applied followed by Tukey multiple comparison tests. *P* value of ≤ 0.05 was considered statistically significant. The entire statistical analyses were performed using SPSS 21.0 software (SPSS Inc., Chicago, IL, USA).

4.5. Computational molecular modeling studies

Computational molecular modeling is an important tool for understanding the mechanisms of molecular interaction between protein targets and inhibitors, which can be fundamental for development of new anti-cancer pharmaceuticals in treatment of many diseases including cancer therapeutics.

4.5.1. Protein Preparation and Grid Generation: -

The 3D coordinates of the tubulin crystal structure were obtained from Protein Data Bank (PDB ID code: 3UT5). The PDB protein-ligand structures were processed with the Protein Preparation Wizard in the Schrödinger suite. The protein structure integrity was checked and adjusted, and missing residues and loop segments near the active site were added using Prime. A 3D box was generated around each ligand to enclose the entire vicinity of active site. The receptor grid was prepared with the help of OPLS_2005 force field. The grid center was set to be the centroid of the co-crystallized ligand, and the cubic grid had a size of 20 Å.

4.5.2. Ligand Preparation: -

3D structures were generated by Schrödinger suite. Schrödinger's LigPrep program was used to generate different conformations of ligands.

4.5.3. Molecular Docking: -

Molecular docking studies were performed by using a GLIDE docking module of Schrödinger suite. For the validation of the docking protocol, the cocrystallized ligand (Colchicine in 3UT5)

was subjected to re-docking into the tubulin dimer (PDB code: 3UT5) using GLIDE. The bound and docked conformations of Colchicine showed similar interactions and binding pose at their respective binding sites. Finally, prepared ligands were docked into the generated receptor grids using Glide SP docking precision. The results were analyzed on the basis of the GLIDE docking score and molecular recognition interactions. The 3D images were generated using Schrödinger Suite 2017-1.

4.5.4. Molecular Docking Protocol Validation:

The docking protocol was validated by redocking of the bound ligand colchicine in the colchicine binding site of tubulin protein using GLIDE module of Schrödinger software. This analysis establishes the acceptability of docking protocol and thus can be extended to dock investigated molecules in the colchicine binding site of tubulin protein.

SUPPORTING INFORMATION:

Additional supplemental figures, videos, experimental procedures and spectroscopic characterization data (^1H & ^{13}C NMR, and HRMS Spectra) of all the synthesized compounds. Molecular formula strings are also available. “This material is available free at journal site.”

Supplementary Figures: Figure S1: Activity oriented phenstatin bearing indole linked chalcones structure representation. Figure S2: Cytotoxic effect of compounds **9a-z** and **9aa-ad** against SCC-29B oral squamous cancer cell line. Figure S3: Cytotoxic effect of compounds against various cancer cell lines. Figure S4: Immunophenotypic characterization of SSC-29B cells. Figure S5: Adriamycin drug uptake in SCC-29B cell line. Figure S6: Acute toxicity of compound **9a** on animal body weight. Figure S7: Effect of conjugate **9a** on tumor reduction of oral cancer xenograft AW13516. Figure S8: Superimposition of compounds **9a** (turquoise) and **9e** (grey) with co-crystal structure (green) colchicine (PDB ID code: 3UT5). Figure S9: Superimposition of bound co-crystal and docked conformation of co-crystal in the colchicine binding site of tubulin (PDB ID code: 3UT5) for validation of docking protocol.

Supplementary Tables: Table S1: Growth Inhibition property of compounds against Oral cancer cell line SCC-29B by *in vitro* cytotoxicity assay. Table S2: Growth Inhibition property of compounds against Liver hepatoma cell line Hep-G2 by *in vitro* cytotoxicity assay. Table S3: Growth Inhibition property of compounds against Colon cancer cell line HT-29 by *in vitro* cytotoxicity assay. Table S4: Maximum tolerated dose evaluation. Table S5: Efficacy against AW13516 Human Oral cancer xenograft (i.v. route). Table S6. GLIDE docking results for **9a** and **9e** at the tubulin binding site of colchicine (PDB ID: 3UT5). Table S7. GLIDE docking results for compound **9a** at the active binding sites of GAPDH (PDB ID: 1U8F), HK 2 (PDB ID: 2NZT), LDH (PDB ID: 1I0Z), PGK (PDB ID: 4AXX), PDH (PDB ID: 3EXE) **and** IDH1 (PDB ID: 4UMX) proteins.

PDB ID Codes: Colchicine (PDB ID: 3UT5)⁵⁵, GAPDH (PDB ID: 1U8F)⁵⁸, HK 2 (PDB ID: 2NZT)⁵⁹, LDH (PDB ID: 1I0Z)⁶⁰, PGK (PDB ID: 4AXX)⁶¹, PDH (PDB ID: 3EXE)⁶² and IDH1 (PDB ID: 4UMX)⁶³.

Use of Animal Subjects:

All procedures involving mice were performed according to protocols approved by Institutional Animal Ethics Committee, ACTREC, Tata Memorial Centre, Navi Mumbai (Proposal # 1/2015) and were adhered to CPCSEA guidelines (Registration Number: 65/GO/ReBiBt/S/99/CPCSEA).

AUTHOR INFORMATION:

Corresponding Authors

*For J.K.: Email: jkode@actrec.gov.in (Jyoti Kode; Biological *in vitro* and *in vivo* studies); Tel: +91-22-27405030; Fax: +91-22-27405085.

*For A.K.: Email: ahmedkamal915@gmail.com (Ahmed Kamal; Design, synthesis and physicochemical studies); Tel. No. +91-11-26059662.

Author Contributions: Jyoti Kode, Jeshma Kovvuri, Burri Nagaraju and Ahmed Kamal contributed equally to this work.

Potential conflicts of interest

The authors declare no conflict of interest.

AUTHORSHIP CONTRIBUTION STATEMENT:

Concept and design: J. Kode (Biological study), A. Kamal (Chemistry study)

Development of methodology, acquisition of data, analysis and interpretation of data: A. Kamal, J. Kovvuri, B. Nagaraju, G. Kumar (Chemistry study), J. Kode, S. Jadhav, Subrata Sen, Nirmal Kumar K., M. Barkume, T. Pradhan (Biological study), P. Chaudhari. Bhabani Shankar Mohanty (PET-CT Imaging), J. Gour, D. Sigalapalli (Molecular Docking study), M. Banerjee (SPR analysis)

Writing, review, and/or revision of the manuscript: J. Kode, A. Kamal.

Financial support: A. Kamal (IICT), J. Kode (ACTREC).

Final approval of the manuscript: J. Kode, A. Kamal and all co-authors.

ACKNOWLEDGEMENT:

Authors would like to thank Council of Scientific and Industrial Research (CSIR), Government of India for financial support under the 12th Five Year plan project “Affordable Cancer Therapeutics” (CSC0301) and “Small Molecules in Lead Exploration (SMiLE)” (CSC0111). Authors J. K. and B. N. are thankful to Department of Science & Technology, New Delhi for providing fellowships under DST-INSPIRE Fellowship programme and CSIR-IICT-Hyderabad. S. J. received SRF fellowship from Council of Scientific & Industrial Research, Government of India. Authors wish to thank Dr Radu Tamaian, SC Biotech Corp SRL, Romania for critical review of manuscript. Authors would like to thank Dr Sorab Dalal, Principal Investigator, Sorab Lab at ACTREC for providing anti-tubulin antibody for performing immunofluorescence assay. Authors wish to thank excellent support extended by Dr Sharada Sawant, Officer-In Charge, Electron Microscopy Facility at ACTREC for providing TEM Imaging data. Authors would like

to acknowledge help received from Flow cytometry facility, Digital Imaging Facility, Laboratory Animal facility and Histology Facility at ACTREC. Authors would like to extend special thanks to Dr Arvind Ingle for reading H & E slides for xenograft tumor sections.

ABBREVIATIONS:

CA-4, combretastatin A-4; CSC, cancer stem-like cells; NE, non-evaluable; NT: non-tested; SRB, Sulforhodamine B; MTS, Masson's Trichrome Staining; SPR: Surface Plasmon Resonance, TCA cycle: Tricarboxylic acid cycle, TEM: Transmission electron microscopy, SUV: standard uptake value, RTV: Relative Tumor Volume, PET-CT: positron emission tomography/computed tomography, HK-2: Hexokinase-2, ^{18}F -FDG: [^{18}F]-fluorodeoxyglucose, GI_{50} : 50% growth inhibition, TGI: total growth inhibition, LC_{50} : 50% lethal concentration, ADR: Adriamycin, DMSO: dimethyl sulfoxide, MTS: Masson's Trichrome stain, MTOC: Microtubule organizing centre, MTD: maximum tolerated dose, i.v.: intravenous

REFERENCES:

- [1] Warnakulasuriya, S. Global Epidemiology of Oral and Oropharyngeal Cancer. *Oral Oncol.* **2009**, *45* (4–5), 309–316. <https://doi.org/10.1016/J.Oraloncology.2008.06.002>.
- [2] McKean, P. G.; Vaughan, S.; Gull, K. The Extended Tubulin Superfamily. *J. Cell Sci.* **2001**, *114* (15), 2723–2733.
- [3] Choi, M. J.; No, E. S.; Thorat, D. A.; Jang, J. W.; Yang, H.; Lee, J.; Choo, H.; Kim, S. J.; Lee, C. S.; Ko, S. Y.; Lee, J.; Nam, G.; Pae, A. N. Synthesis and Biological Evaluation of Aryloxazole Derivatives as Antimitotic and Vascular-Disrupting Agents for Cancer Therapy. *J. Med. Chem.* **2013**, *56*, 9008–9018. <https://doi.org/10.1021/jm400840p>
- [4] Flynn, B. L.; Gill, Gurmit, S.; Grobelny, D. W.; Chaplin, J. H.; Paul, D.; Leske, A. F.; Lavranos, T. C.; Chalmers, D. K.; Charman, S. A.; Kostewicz, E.; Shackelford, D. M.; Morizzi, J.; Hamel, E.; Jung, M. K.; Kremmidiotis, G. Discovery of 7-Hydroxy-6-methoxy-2-methyl-3-(3,4,5-trimethoxybenzoyl)benzo[b]furan (BNC105), a Tubulin Polymerization Inhibitor with Potent Antiproliferative and Tumor Vascular Disrupting

- Properties. *J. Med. Chem.* **2011**, *54*, 6014–6027. <https://doi.org/10.1021/jm200454y>
- [5] Lee, R. M.; Gewirtz, D. A. Colchicine Site Inhibitors of Microtubule Integrity as Vascular Disrupting Agents. *Drug Dev. Res.* **2008**, *69*, 352–358. <https://doi.org/10.1002/ddr.20267>
- [6] Kaul, R.; Risinger, A. L.; Mooberry, S. L. Microtubule-Targeting Drugs: More than Antimitotics. *J. Nat. Prod.* **2019**, *82* (3), 680–685. <https://doi.org/10.1021/acs.jnatprod.9b00105>.
- [7] Comess, K. M.; McLoughlin, S. M.; Oyer, J. A.; Richardson, P. L.; Stöckmann, H.; Vasudevan, A.; Warder, S. E. Emerging Approaches for the Identification of Protein Targets of Small Molecules-A Practitioners' Perspective. *J. Med. Chem.* **2018**, *61* (19), 8504–8535. <https://doi.org/10.1021/acs.jmedchem.7b01921>.
- [8] Li, W., Sun, H., Xu, S., Zhu, Z., & Xu, J. (in press). Tubulin inhibitors targeting the colchicine binding site: a perspective of privileged structures. *Future Med Chem*, **2017**, *9* (15), 1765-1794. <https://doi.org/10.4155/fmc-2017-0100>.
- [9] Arnst, K. E.; Wang, Y.; Lei, Z.-N.; Hwang, D.-J.; Kumar, G.; Ma, D.; Parke, D. N.; Chen, Q.; Yang, J.; White, S. W.; Seagroves, T. N.; Chen, Z.-S.; Miller, D. D.; Li, W. Colchicine Binding Site Agent DJ95 Overcomes Drug Resistance and Exhibits Antitumor Efficacy. *Mol Pharmacol.* **2019**, *96* (1), 73-89. <https://doi.org/10.1124/mol.118.114801>.
- [10] McLoughlin, E. C.; and O'Boyle, N. M. Colchicine-Binding Site Inhibitors from Chemistry to Clinic: A Review. *Pharmaceuticals (Basel)* **2020**, *13* (4) 72; <https://doi.org/10.3390/ph13010008>.
- [11] Brito, D. A.; Yang, Z.; Rieder, C. L. Microtubules Do Not Promote Mitotic Slippage When the Spindle Assembly Checkpoint Cannot Be Satisfied. *J. Cell Biol.* **2008**, *182* (4), 623–629. <https://doi.org/10.1083/jcb.200805072>.
- [12] Ravelli, R. B. G.; Gigant, B.; Curmi, P. A.; Jourdain, I.; Lachkar, S.; Sobel, A.; Knossow, M. Insight into Tubulin Regulation from a Complex with Colchicine and a Stathmin-like Domain. *Nature* **2004**, *428* (6979), 198–202. <https://doi.org/10.1038/nature02393>.
- [13] Lu, Y.; Chen, J.; Xiao, M.; Li, W.; Miller, D. D. An Overview of Tubulin Inhibitors That Interact with the Colchicine Binding Site. *Pharm. Res.* **2012**, *29*, 2943–2971.

<https://doi.org/10.1007/s11095-012-0828-z>

- [14] Chaudhary, A.; Pandeya, S. N.; Kumar, P.; Sharma, P. P.; Gupta, S.; Soni, N.; Verma K. K.; Bhardwaj, G. Combretastatin A-4 Analogs as Anticancer Agents. *Mini-Rev. Med. Chem.* **2007**, *7* (12) 1186-1205. <https://doi.org/10.2174/138955707782795647>.
- [15] Pettit, G. R.; Singh, S. B.; Hamel, E.; Lin, C. M.; Alberts, D. S.; Garcia-Kendal, D. Isolation and structure of the strong cell growth and tubulin inhibitor combretastatin A-4. *Experientia.* **1989**, *45*, 209–211. <https://doi.org/10.1007/BF01954881>
- [16] Kamal, A.; Kumar, G. B.; Vishnuvardhan, M. V. P. S.; Shaik, A. B.; Reddy, V. S.; Rasala M.; Sayeeda, I. B.; Kapure, J. S. Synthesis of phenstatin/isocombretastatin-chalcone conjugates as potent tubulin polymerization inhibitors and mitochondrial apoptotic inducers. *Org. Biomol. Chem.*, **2015**, *13* (13), 3963-3981. <https://doi.org/10.1039/C4OB02606C>.
- [17] Pettit, G. R.; Toki, B.; Herald, D. L.; Verdier-Pinard, P.; Boyd, M. R.; Hamel, E.; Pettit, R. K. Antineoplastic agents. 379. Synthesis of phenstatin phosphate. *J. Med. Chem.* **1998**, *41*(10), 1688-1695. <https://doi.org/10.1021/jm970644q>.
- [18] Li, Q.; Jian, X.-E.; Chen, Z.-R.; Chen, L.; Huo, X.-S.; Li, Z.-H.; You, W.-W.; Rao, J.-J.; Zhao, P.-L. Synthesis and biological evaluation of benzofuran-based 3,4,5-trimethoxybenzamide derivatives as novel tubulin polymerization inhibitors. *Bioorg. Chem.* **2020**, *102*, 104076. <https://doi.org/10.1016/j.bioorg.2020.104076>
- [19] Chiang, N.-J.; Shiah, H.-S.; Lin, C.-C.; Yen, C.-J.; Tsai, H.-J. Wu, S.-Y.; Su, W.-C.; Chang, K.-Y. Chen, L.-T. A phase I dose escalation study of SCB01A, a micro-tubular inhibitor with vascular disrupting activity, in patients with advanced solid tumors refractory to standard therapy. *J. Clin. Oncol.* **2017**, *35* (15), 2531-2531. <https://doi.org/10.1200/JCO.2017.35.15>.
- [20] Kuo, C.-C.; Hsieh, H.-P.; Pan, W.-Y.; Chen, C.-P.; Liou, J.-P.; Lee, S.-J.; Chang, Y.-L.; Chen, L.-T.; Chen, C.-T.; Chang, J.-Y. BPR0L075, a Novel Synthetic Indole Compound with Antimitotic Activity in Human Cancer Cells, Exerts Effective Antitumoral Activity *in Vivo*. *Cancer Res.* **2004**, *64*, 4621–4628.
- [21] Patil, R.; Patil, S. A.; Beaman, K. D.; Patil, S. A. Indole molecules as inhibitors of tubulin polymerization: potential new anticancer agents, an update (2013-2015). *Future*

Med Chem **2016**, *8* (11),1291-316. <https://doi.org/10.4155/fmc-2016-0047>

- [22] Romagnoli, R.; Baraldi, P. G.; Sarkar, T.; Carrion, M. D.; Cara, C. L.; Cruz-Lopez, O.; Preti, D.; Tabrizi, M. A.; Tolomeo, M.; Grimaudo, S.; Cristina, A. D.; Zonta, N.; Balzarini, J.; Brancale, A.; Hsieh, H.-P.; Hamel, E. Synthesis and Biological Evaluation of 1-Methyl-2-(3',4',5'-trimethoxybenzoyl)-3-aminoindoles as a New Class of Antimitotic Agents and Tubulin Inhibitors. *J. Med. Chem.* **2008**, *51*, 1464–1468.
- [23] Liou, J.-P.; Chang, Y.-L.; Kuo, F.-M.; Chang, C.-W.; Tseng, H.-Y.; Wang, C.-C.; Yang, Y.-N.; Chang, J.-Y.; Lee, S.-J.; Hsieh, H.-P. Concise Synthesis and Structure-Activity Relationships of Combretastatin A-4 Analogues, 1-Aroylindoles and 3-Aroylindoles, as Novel Classes of Potent Antitubulin Agents. *J. Med. Chem.* **2004**, *47*, 4247-4257.
- [24] Hadimani, M. B.; MacDonough, M. T.; Ghatak, A.; Strecker, T. E.; Lopez, R.; Sriram, M.; Nguyen, B. L.; Hall, J. J.; Kessler, R. J.; Shirali, A. R.; Liu, L.; Garner, C. M.; Pettit, G. R.; Hamel, E.; Chaplin, D. J.; Mason, R. P.; Trawick, M. L.; Pinne, K. G. Synthesis of a 2-Aryl-3-aryl Indole Salt (OXi8007) Resembling Combretastatin A-4 with Application as a Vascular Disrupting Agent. *J. Nat. Prod.* **2013**, *76*, 1668–1678.
- [25] Lia, L.; Jiangb, S.; Lic, X.; Liud, Y.; Sue, J.; Chen, J. Recent advances in trimethoxyphenyl (TMP) based tubulin inhibitorstargeting the colchicine binding site. *Eur. J. Med. Chem.* **2018**, *151*, 482-494. <https://doi.org/10.1016/j.ejmech.2018.04.011>
- [26] Do, C.V.; Faouzi, A.; Barette, C.; Farce, A.; Fauvarque, M.O.; Colomb, E.; Catry, L.; Berthier-Vergnes, O.; Haftek, M.; Barret, R.; et al. Synthesis and biological evaluation of thiophene and benzo b thiophene analogs of combretastatin A-4 and isocombretastatin A-4: A comparison between the linkage positions of the 3,4,5-trimethoxystyrene unit. *Bioorg. Med. Chem. Lett.* **2016**, *26*, 174–180. <https://doi.org/10.1016/j.bmcl.2015.11.010>.
- [27] Zhuang, C.; Zhang, W.; Sheng, C.; Zhang, W.; Xing, C.; Miao, Z. Chalcone: A Privileged Structure in Medicinal Chemistry. *Chem. Rev.* **2017**, *117* (12), 7762–7810. <https://doi.org/10.1021/acs.chemrev.7b00020>.
- [28] Aroraa, S.; Gonzalez b, A. F.; Solankia, K. Combretastatin A-4 and its Analogs in Cancer Therapy. *Int. J. Pharm. Sci. Rev. Res.* **2013**, *22* (2), 168-174.
- [29] Woods, J.; Hadfield, J.; Pettit, G.; Fox, B.; McGown, A. The Interaction with Tubulin of

- a Series of Stilbenes Based on Combretastatin A-4. *Br. J. Cancer* **1995**, *71* (4), 705–711. <https://doi.org/10.1038/bjc.1995.138>.
- [30] Álvarez, R.; Puebla, P.; Díaz, J. F.; Bento, A. C.; García-Navas, R.; Iglesia-Vicente, J.; Mollinedo, F.; Andreu, J. M.; Medarde, M.; Peláez, R. Endowing Indole-Based Tubulin Inhibitors with an Anchor for Derivatization: Highly Potent 3-Substituted Indole Phenstatins and Isocombretastatins. *J. Med. Chem.* **2013**, *56*, 2813–2827.
- [31] Dhanya, S.; Pooja, K.; R. Indole based Tubulin Polymerization Inhibitors: An Update on Recent Developments. *Mini Rev. Med. Chem.* **2016**, *16* (18), 1470–1499.
- [32] Agents, A.; Mahboobi, S.; Pongratz, H.; Hufsky, H.; Frieser, M.; Lyssenko, A.; Paper, D. H.; Bu, J.; Bo, F. Synthetic 2-Aroylindole Derivatives as a New Class of Potent Tubulin-Inhibitory, Antimitotic Agents. *J. Med. Chem.* **2001**, *44* (i), 4535–4553. <https://doi.org/10.1021/jm010940>.
- [33] Zdrazil, B.; Guha, R. The Rise and Fall of a Scaffold: A Trend Analysis of Scaffolds in the Medicinal Chemistry Literature. *J. Med. Chem.* **2018**, *61* (11), 4688–4703. <https://doi.org/10.1021/acs.jmedchem.7b00954>.
- [34] Yan, J.; Chen, J.; Zhang, S.; Hu, J.; Huang, L.; Li, X. Synthesis, Evaluation and Mechanism Study of Novel Indole Chalcone Derivatives Exerting Effective Antitumor Activity Through Microtubule Destabilization in Vitro and in Vivo. *J. Med. Chem.* **2016**, *59*, 5264–5283.
- [35] Mirzaei, H.; Shokrzadeh, M.; Modanloo, M.; AliZiar, Riazi, G. H.; Emami, S. New indole-based chalconoids as tubulin-targeting antiproliferative agents. *Bioorg. Chem.* **2017**, *75*, 86–98. <https://doi.org/10.1016/j.bioorg.2017.09.005>.
- [36] Zhu, C.; Zuo, Y.; Wang, R.; et al., Discovery of potent cytotoxic ortho-aryl chalcones as new scaffold targeting tubulin and mitosis with affinity-based fluorescence, *J. Med. Chem.* **2014**, *57*, 6364–6382.
- [37] Dyrager, C.; Wickström, M.; Fridén-Saxin, M.; Friberg, A.; Dahlén, K.; Wallén, E. A. A.; Gullbo, J.; Grøtli, M.; Luthman, K. Inhibitors and promoters of tubulin polymerization: Synthesis and biological evaluation of chalcones and related dienonesas potential anticancer agents. *Bioorg. Med. Chem.* **2011**, *19*, 2659–2665. <https://doi.org/10.1016/j.bmc.2011.03.005>.

- [38] Cong, H.; Zhao, X.; Castle, B. T.; Pomeroy, E. J.; Zhou, B.; Lee, J.; Wang, Y.; Bian, T.; Miao, Z.; Zhang, W.; Sham, Y. Y.; Odde, D. J.; Eckfeldt, C. E.; Xing, C.; Zhuang, C. An indole-chalcone inhibits multidrug-resistant cancer cell growth by targeting microtubules. *Mol. Pharmaceutics*, **2018**, *15*, 3892–3900. <https://doi.org/10.1021/acs.molpharmaceut.8b00359>
- [39] Singh p.; Anand, A.; Kumar, V. Recent developments in biological activities of chalcones: A mini review. *Eur. J. Med. Chem.* **2014**, *85*, 758-777. <https://doi.org/10.1016/j.ejmech.2014.08.033>
- [40] Infante, P.; Alfonsi, R.; Ingallina, C.; Quaglio, D.; Ghirga, F.; D'Acquarica, I.; Bernardi, F.; Di Magno, L.; Canettieri, G.; Screpanti, I.; et al. Inhibition of Hedgehog-Dependent Tumors and Cancer Stem Cells by a Newly Identified Naturally Occurring Chemotype. *Cell Death Dis.* **2016**, *7* (9), e2376. <https://doi.org/10.1038/cddis.2016.195>
- [41] Ashraf, Md.; Thokhir, B.S; Malik, M.S; Syed, R; Mallipeddi, P.L; Vishnuvardhan, M.V.P.S; Kamal, A., Design and synthesis of cis-restricted benzimidazole and benzothiazole mimics of combretastatin A-4 as antimitotic agents with apoptosis inducing ability. *Bioorg. Med. Chem. Lett.*, 2016, *26*, 4527.
- [42] Jadala C.; Sathish, M; Anchi, P.; Tokala, R.; Lakshmi, U.J.; Ganga, R.; Shankaraiah, N.; Godugu, C.; Kamal, A., Synthesis of combretastatin-A4 carboxamides that mimicsulfonyl piperazines by a molecular hybridization approach: in vitro cytotoxicity evaluation and inhabitation of tubulin polymerization. *ChemMedChem.*, 2019, *14*, 2052.
- [43] Kamal, A; Kumar, G.B; Vishnuvardhan, M.V.P.S; Shaik, A.B; Reddy, V.S; Mahesh, R; Sayeeda, I.B; Kapure. Synthesis of phenstatin/isocombretastatin–chalcone conjugates as potent tubulin polymerization inhibitors and mitochondrial apoptotic inducers. *J.S., Org. Biomol. Chem.*, 2015, *13*, 3963.
- [44] Narsimha, R.M.P.; Nagarju, B.; Jeshma, K.; Vishnuvardhan, M.V.P.S.; Pollepalli, S.; Jain, N.; Kamal, A., Synthesis of imidazo-thiadiazole linked indolinone conjugates and evaluated their microtubule network disrupting and apoptosis inducing ability. *Bioorg. Chem.*, 2018, *76*, 420.
- [45] Miao, Y.; Zhang, L.; Guo, R.; Liang, S.; Zhang, M.; Shi, S.; Shang-Guan, C.-F.; Liu, M.-F.; Li, B. 18F-FDG PET/CT for Monitoring the Response of Breast Cancer to MiR-

- 143-Based Therapeutics by Targeting Tumor Glycolysis. *Mol. Ther. - Nucleic Acids* **2016**, *5* (8), e357. doi: 10.1038/mtna.2016.72.
- [46] Yadav, S; Pandey, S. K; Singh, V. K; Goel, Y; Kumar, A; Singh, S. M., Molecular docking studies of 3-bromopyruvate and its derivatives to metabolic regulatory enzymes: Implication in designing of novel anticancer therapeutic strategies. *PLoS One*. **2017**, *12*, e0176403.
- [47] Dogra N.; Kumar A.; Mukhopadhyay T. Fenbendazole acts as a moderate microtubule destabilizing agent and causes cancer cell death by modulating multiple cellular pathways. *Sci Rep*. 2018, 8(1), 11926. doi:10.1038/s41598-018-30158-6
- [48] Ghuwalewala, S.; Ghatak, D.; Das, P.; Dey, S.; Sarkar, S.; Alam, N.; Panda, C. K.; Roychoudhury, S. CD44 High CD24 Low Molecular Signature Determines the Cancer Stem Cell and EMT Phenotype in Oral Squamous Cell Carcinoma. *Stem Cell Res*. **2016**, *16* (2), 405–417. <https://doi.org/10.1016/j.scr.2016.02.028>.
- [49] Apgar, J. M.; Juarranz, A.; Espada, J.; Villanueva, A.; Cañete, M.; Stockert, J. C. Fluorescence Microscopy of Rat Embryo Sections Stained with Haematoxylin-Eosin and Masson's Trichrome Method. *J. Microsc.* **1998**, *191* (Pt 1), 20–27.
- [50] Moores, C. Studying Microtubules by Electron Microscopy. *Methods Cell Biol.*, **2008**, *88*, 299-317. [https://doi.org/10.1016/S0091-679X\(08\)00416-0](https://doi.org/10.1016/S0091-679X(08)00416-0)
- [51] Manka, S. W.; Moores, C. A. The role of tubulin–tubulin lattice contacts in the mechanism of microtubule dynamic instability. *Nature Structural & Molecular Biology*. 2018 <https://doi.org/10.1038/s41594-018-0087-8>
- [52] Li, Q.; Jian, X-E.; Chen, Z-R.; Chen, L.; Huo, X-S.; Li, Z-H.; You, W-W.; Rao, J-J.; Zhao, P-L.; Synthesis and biological evaluation of benzofuran-based 3,4,5-trimethoxybenzamide derivatives as novel tubulin polymerization. *Bioorg. Chem*. **2020**, *102*, 104076. <https://doi.org/10.1016/j.bioorg.2020.104076>
- [53] Folker, E. S.; Baker, B. M.; Goodson, H. V. Interactions between CLIP-170, Tubulin, and Microtubules: Implications for the Mechanism of CLIP-170 Plus-End Tracking Behavior D V. *Molecular Biology of the Cell*. Vol. 16, 5373–5384, November 2005.
- [54] Vergez, S.; Delord, J.-P.; Thomas, F.; Rochaix, P.; Caselles, O.; Filleron, T.; Brillouet, S.; Canal, P.; Courbon, F.; Allal, B. C. Preclinical and Clinical Evidence That Deoxy-2-

- [18F]Fluoro-D-Glucose Positron Emission Tomography with Computed Tomography Is a Reliable Tool for the Detection of Early Molecular Responses to Erlotinib in Head and Neck Cancer. *Clin. Cancer Res.* **2010**, *16* (17), 4434–4445. <https://doi.org/10.1158/1078-0432.CCR-09-2795>.
- [55] Ranaivoson, F. M.; Gigant, B.; Berritt, S.; Joullie, M.; Knossow, M. Structural plasticity of tubulin assembly probed by vinca-domain ligands. *Acta Cryst.* 2012, *D68*, 927.
- [56] Schrödinger suite 2014-3; Schrödinger, LLC: New York, 2014.
- [57] Nakagawa-Goto, K.; Oda, A.; Hamel, E.; Ohkoshi, E.; Lee, K.-H. Goto, M. Development of a novel class of tubulin inhibitor from desmosmumotin B with a hydroxylated bicyclic B-ring. *J. Med. Chem.*, 2015, *58*, 2378.
- [58] Jenkins, J. L.; Tanner, J. J. High-resolution structure of human D-glyceraldehyde-3-phosphate dehydrogenase. *Acta Crystallogr., Sect. D*, **2006**, *62*, 290-301.
- [59] [https://www.rcsb.org/structure/2NZT\(10.2210/pdb2NZT/pdb\)](https://www.rcsb.org/structure/2NZT(10.2210/pdb2NZT/pdb))
- [60] Read, J. A.; Winter, V. J.; Eszes, C. M.; Sessions, R. B.; Brady, R. L., Structural basis for altered activity of M- and H-isozyme forms of human lactate dehydrogenase. *Proteins*, **2001**, *43*, 175-185.
- [61] <https://www.rcsb.org/structure/4AXX> (DOI: 10.2210/pdb4AXX/pdb)
- [62] Kato, M.; Wynn, R.M.; Chuang, J. L.; Tso, S.C.; Machius, M.; Li, J.; Chuang, D. T., Structural basis for inactivation of the human pyruvate dehydrogenase complex by phosphorylation: role of disordered phosphorylation loops. *Structure*, **2008**, *16*, 1849-1859.
- [63] Deng, G.; Shen, J.; Yin, M.; Mcmanus, J.; Mathieu, M.; Gee, P.; He, T.; Shi, C.; Bedel, O.; Mclean, L. R.; Le-Strat, F.; Zhang, Y.; Marquette, J.; Gao, Q.; Zhang, B.; Rak, A.; Hoffmann, D.; Rooney, E.; Vassort, A.; Englaro, W.; Li, Y.; Patel, V.; Adrian, F.; Gross, S.; Wiederschain, D.; Cheng, H.; Licht, S., Selective Inhibition of Mutant Isocitrate Dehydrogenase 1 (Idh1) Via Disruption of a Metal Binding Network by an Allosteric Small Molecule. *J. Biol. Chem.* **2015**, *290*, 762-774.
- [64] Rai, G.; Brimacombe, K.R.; Mott, B.T. , Urban, D.J.; Hu, X.; Yang, S-M, Lee, T.D.; Cheff, D.M.; Kouznetsova, J.; Benavides, G.; Pohida, K.; Kuenstner, E.; Luci, D.; Lukacs, C.; Davies, D.; Dranow, C.; Zhu, H.; Sulikowski, G.; Moore, W.; Stott, G.;

- Flint, A.; Hall, M.; Darley-USmar, V.; Neckers, L.; Dang, C.; Waterson, A.; Simeonov, A.; Jadhav, A.; Maloney, D. Discovery and Optimization of potent, cell-active pyrazole-based inhibitors of Lactate Dehydrogenase (LDH). *J. Med Chem.* 2017, 60: 9184–9204.
- [65] Skehan, P.; Storeng, R.; Scudiero, D.; Monks, A.; McMahon, J.; Vistica, D.; Warren, J. T.; Bokesch, H.; Kenney, S.; Boyd, M. R. New Colorimetric Cytotoxicity Assay for Anticancer-Drug Screening. *J. Natl. Cancer Inst.* **1990**, 82 (13), 1107–1112. <https://doi.org/10.1093/jnci/82.13.1107>.
- [66] Shaik, A. B.; Rao, G. K.; Kumar, G. B.; Patel, N.; Reddy, V. S.; Khan, I.; Routhu, S. R.; Kumar, C. G.; Veena, I.; Chandra Shekar, K.; et al. Design, Synthesis and Biological Evaluation of Novel Pyrazolochalcones as Potential Modulators of PI3K/Akt/MTOR Pathway and Inducers of Apoptosis in Breast Cancer Cells. *Eur. J. Med. Chem.* **2017**, 139, 305–324. <https://doi.org/10.1016/j.ejmech.2017.07.056>.
- [67] Deng, R.; Wang, X.; Liu, Y.; Yan, M.; Hanada, S.; Xu, Q.; Zhang, J.; Han, Z.; Chen, W.; Zhang, P. A New Gamboge Derivative Compound 2 Inhibits Cancer Stem-like Cells via Suppressing EGFR Tyrosine Phosphorylation in Head and Neck Squamous Cell Carcinoma. *J. Cell. Mol. Med.* **2013**, 17 (11), 1422–1433. <https://doi.org/10.1111/jcmm.12129>.
- [68] Geran, R. S.; Greenberg, N. H.; Macdonald, M. M.; Schumacher, A. M.; Abbott, B. J. Protocol 4: Selection of Dosage. In *Protocols for Screening Chemical Agents and Natural Products against Animal Tumors and Other Biological Systems. Cancer Chemotherapy Reports Part 3*; National Cancer Institute; Division of Cancer Treatment; National Institutes of Health: Bethesda, 1972; p 46.
- [69] Kholiya, F.; Chatterjee, S.; Bhojani, G.; Sen, S.; Barkume, M.; Kasinathan, N. K.; Kode, J.; Meena, R. Seaweed polysachharide derived bioaldehyde nanocomposite: Potential application in anticancer therapeutics. *Carbohydrate Polymers.* **2020**, 240 (15), 116282. doi.org/10.1016/j.carbpol.2020.116282. 2020.
- [70] Geran, R. S.; Greenberg, N. H.; Macdonald, M. M.; Schumacher, A. M.; Abbott, B. J. Protocol 11: Test Evaluation. In *Protocols for Screening Chemical Agents and Natural Products against Animal Tumors and Other Biological Systems. Cancer Chemotherapy Reports Part 3*; National Cancer Institute; Division of Cancer Treatment; National

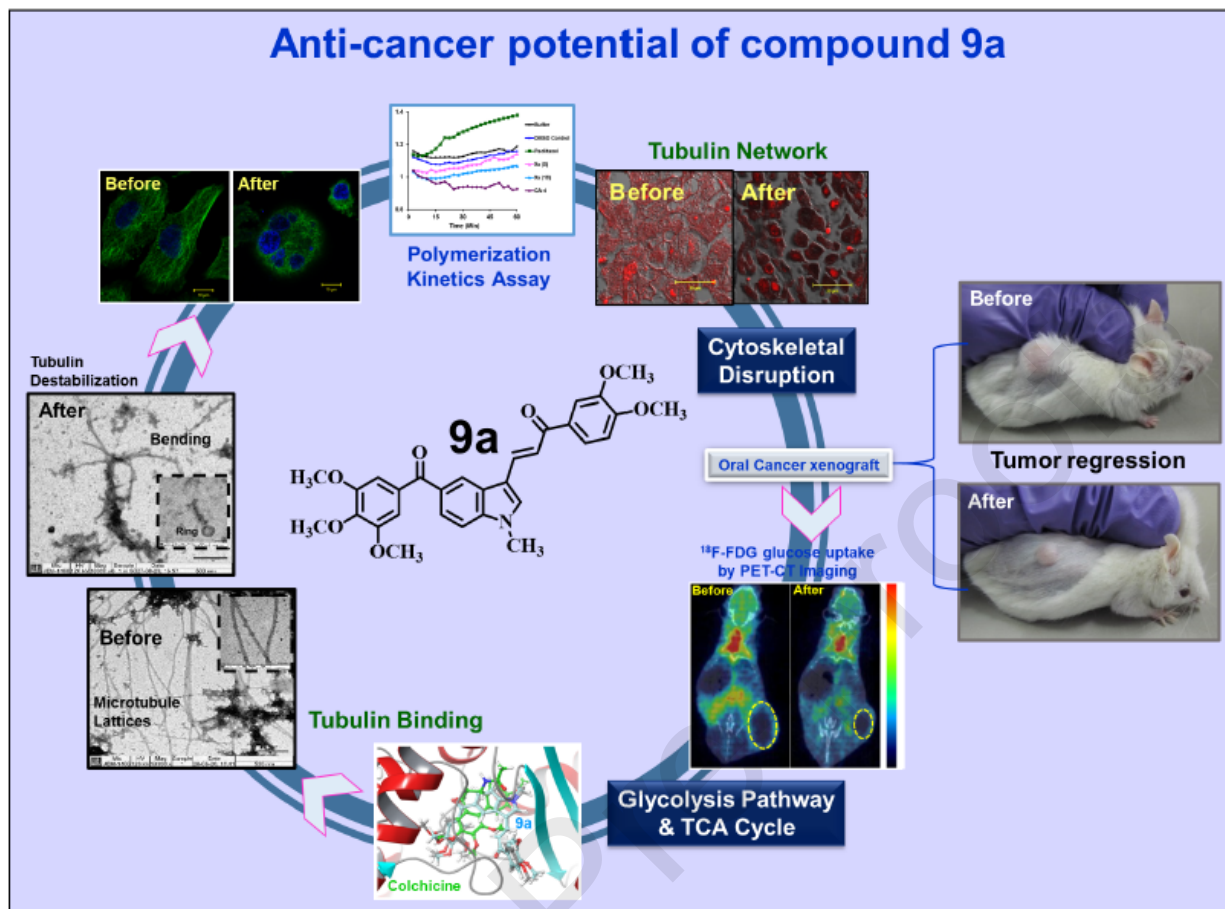
Institutes of Health: Bethesda, 1972; p 25.

- [71] Holbeck, S. L.; Collins, J. M.; Doroshow, J. H. Analysis of Food and Drug Administration-Approved Anticancer Agents in the NCI60 Panel of Human Tumor Cell Lines. *Mol. Cancer Ther.* **2010**, *9* (5), 1451–1460. <https://doi.org/10.1158/1535-7163.mct-10-0106>.
- [72] Banerjee M, Chakravarty D, Ballal A. Molecular basis of function and the unusual antioxidant activity of a cyanobacterial cysteine desulfurase. *Biochem J.* **2017**, *474* (14), 2435-2447. <https://doi.org/10.1042/BCJ20170290>

Declaration of interests

The authors declare that they have no known competing financial interests or personal relationships that could have appeared to influence the work reported in this paper.

The authors declare the following financial interests/personal relationships which may be considered as potential competing interests:



HIGHLIGHTS:

- Design and synthesis of “phenstatin-chalcone” analogues **9a-9z** and **9aa-9ad**.
- Biological evaluation of cell cytotoxicity against three cancer cell lines.
- Compound **9a** exhibited antiproliferative activity against 3D spheroids of oral cancer and tumour growth delay in *in vivo* xenograft model.
- Compound **9a** having 1-methyl, 2- and 3-methoxy substituents in aromatic ring exhibited dose-dependent inhibition kinetics of tubulin polymerization.
- Surface Plasmon Resonance analysis confirmed molecular interactions between tubulin and compound **9a**.
- Laser confocal microscopy and electron microscopy validated the destabilization of tubulin assembly by **9a** in oral cancer cells that led to the loss of cell integrity and architecture.
- **9a** significantly reduced fluorodeoxyglucose uptake by oral cancer xenograft leading to tumour reduction.
- Molecular modelling predicted strong interaction and binding of **9a** at colchicine binding site of tubulin and multiple metabolic targets of glucose metabolism pathway.